Geomorphology 276 (2017) 37–50

Contents lists available at ScienceDirect

Geomorphology

journal homepage: www.elsevier.com/locate/geomorph

Decoding the role of tectonics, incision and lithology on drainage divide migration in the Mt. Alpi region, southern Apennines, Italy

J.T. Buscher [a,b,*], A. Ascione [c], E. Valente [d]

[a] Andean Geothermal Center of Excellence (CEGA), Universidad de Chile, Plaza Ercilla 803, Santiago, Chile
[b] Department of Geology, Facultad de Ciencias Físicas y Matemáticas, Universidad de Chile, Plaza Ercilla 803, Santiago, Chile
[c] Dipartimento di Scienze della Terra, dell'Ambiente e delle Risorse, University of Naples Federico II, Largo San Marcellino 10, 80138 Naples, Italy
[d] Dipartimento di Scienze Umanistiche, Sociali e della Formazione, Università del Molise, Campobasso, Italy

ARTICLE INFO

Article history:
Received 21 April 2016
Accepted 5 October 2016
Available online 6 October 2016

Keywords:
Southern Apennines
Drainage divide migration
Stream length-gradient index
Steepness index
Stream convexity
First-order channel gradient index

ABSTRACT

The proclivity of river networks to progressively carve mountain surfaces and preserve markers of landscape adjustments has made analyses of fluvial systems fundamental for understanding the topographic development of orogens. However, the transient nature of uplift and erosion has posed a challenge for inferring the roles that tectonics and/or climate have played on generating topographic relief. The Mt. Alpi region in the southern Apennines has a heterogeneous distribution of elevated topography, erosionally-resistant lithology and uplift, making the area optimal for conducting topographic and river analyses to better understand the landscape development of a transient orogen. Stream length-gradient, normalized channel steepness, stream convexity and first-order channel gradient indices from 10 m digital elevation data from the region exhibit stream profile inconsistencies along the current drainage divide and a dominance of high values subparallel but inboard of the primary chain axis irrespective of known transient landscape factors, suggesting that the current river network may be in a state of transition. The location of these stream profile anomalies both near the modern drainage divide and subparallel to an isolated swath of high topography away from catchment boundaries is thought to be the topographic expression of an imminent drainage divide migration driven primarily by the ~northeast-vergent extension of the western chain axis.

1. Introduction

Tectonic and climatic processes are generally accepted as the primary drivers for building mountainous landscapes (e.g., Molnar and England, 1990), but isolating the role of individual processes responsible for creating orogens that operate at varying spatial and temporal scales has proven to be challenging. The ability of river networks to preserve distinct topographic features created in response to local short-lived surface changes and/or regional long-term external processes has helped in identifying factors that modulate mountainous topography (Whipple and Tucker, 1999; Snyder et al., 2000; Whipple, 2004; Wobus et al., 2006; Whittaker et al., 2008; Di Biase and Whipple, 2011; Whittaker, 2012). River network development primarily depends on how much sediment discharge (climate), large-scale vertical motion (tectonics), and river substrate strength (lithology) affect the river system (Whipple and Tucker, 1999; Snyder et al., 2000; Whipple, 2001; Whipple, 2004; Wobus et al., 2006; Whittaker et al., 2008; Di Biase and Whipple, 2011; Whittaker, 2012), which ultimately characterizes a river as being detachment-limited (i.e. more prone to incision due to minimal sediment coverage), transport-limited (i.e. less prone to incision due to maximal sediment coverage) or a mixture of these two end-members (e.g., Howard, 1994; Willgoose, 1994; Tucker and Slingerland, 1996; Tucker and Whipple, 2002; Whipple and Tucker, 2002; Attal et al., 2011). Profiles of individual rivers provide a first-order snap-shot of the entire river path from headwater to outlet, with deviations from a steady-state graded profile (i.e. concave-up; Flint, 1974) signifying that river incision has not kept pace with external forces such as tectonics and/or climate (e.g., Whipple et al., 1999; Kirby and Whipple, 2001; Lavé and Avouac, 2001; Whipple and Tucker, 2002; Kirby et al., 2003; Duvall et al., 2004; Zaprowski et al., 2005; Wobus et al., 2006).

The transmission of surface perturbations along bedrock rivers due to local or external forcing can collectively alter drainage networks at the catchment scale, ultimately affecting the stability of drainage divides as demonstrated by modelling studies (e.g., Willett et al., 2001, 2014; Pelletier, 2004; Bonnet, 2009; Perron et al., 2012). Drainage divides may experience short-term horizontal mobility in response to changes in base-level (e.g., Prince et al., 2011) or climatic forcing (e.g., Stark, 2010), as well as long-term migration due to normal faulting propagation at rift margins (e.g., Summerfield, 1991; Gilchrist et al., 1994; Tucker and Slingerland, 1994), topographic advection (e.g., Willett et al., 2001; Willett and Brandon, 2002; Miller and Slingerland, 2006; Ramsey et al., 2007) and/or orographic precipitation (e.g.,

* Corresponding author.
E-mail address: jbuscher@ing.uchile.cl (J.T. Buscher).

http://dx.doi.org/10.1016/j.geomorph.2016.10.003
0169-555X/

Willett, 1999; Roe et al., 2003; Anders et al., 2008). The differential influence of tectonic and erosional processes may lead to a drainage divide migration that is out-of-phase with the main topographic crest of a mountain belt, leading to a physical separation of the two at the orogen scale. The movement of the drainage divide away from the crest of maximum peak elevations, where the primary orogen drainage divide is expected, has been shown to be induced by the propagation of deformation within extensional settings and fold and thrust belts (e.g., D'Agostino et al., 2001; Forte et al., 2015).

The decoupling of topographic and drainage network development has also been observed in the southern Apennines of Italy (Amato et al., 1995; Salustri Galli et al., 2002), which has been subject to both NE-verging orogenic transport and extensional faulting. The goal of this study is to help understand the progressive development of the drainage divide in the Mt. Alpi area of the southern Apennines through the interpretation of gross topographic and stream profile features together with analyses of stream profile gradient, steepness and convexity.

2. Tectonic background

The southern Apennines in the Mt. Alpi region are a northeast driven fold-and-thrust belt created by the subduction of the Adria Plate beneath Eurasia (Malinverno and Ryan, 1986) that represent the sum of compressional and extensional tectonics controlled by both thin- and thick-skinned deformation (e.g., Patacca et al., 1990; Cello and Mazzoli, 1998; Patacca and Scandone, 2001; Butler et al., 2004; Shiner et al., 2004; Scrocca et al., 2005; Schiattarella et al., 2006; Mazzoli et al., 2008, 2014). In the late Miocene, back-arc extension of the Tyrrhenian Sea (e.g., Kastens et al., 1988; Faccenna et al., 1996, 1997) occurred concurrently with thin-skinned thrust faulting of the Lagonegro, Apennine Platform and Ligurian Units currently exposed in the Mt. Alpi area, which generated a tectonic wedge (e.g. Sgrosso, 1988; Cello and Mazzoli, 1998; Mazzoli et al., 2014). Back-arc extension trending ~eastward caused down-faulting of blocks, leading to the formation of large coastal grabens that punctuated the southwestern margin of the southern Apennines in the Early Pleistocene (e.g., Sartori, 1990; Savelli and Schreider, 1991).

Starting in the Messinian, the formerly submerged wedge was thrust onto the Apulian Platform (e.g., Butler et al., 2004), above sea level (Ascione and Cinque, 1999), followed by the formation of shallow-water to continental wedge-top basins on top of the Apennine allochthonous units starting in the late part of the Early Pliocene (Mazzoli et al., 2012). Basin subsidence due to slab tear within the down-going Apulian lithosphere followed a progressive southeastward path from c. 4 to c. 2.8 Ma, when the youngest basin (Sant'Arcangelo basin) was formed (Ascione et al., 2012). Uplift of the Nocara anticlinal ridge from the contraction of the structurally lower Apulian Platform (Zuppetta et al., 2004; Capalbo et al., 2010; Mazzoli et al., 2012; Ascione et al., 2012; Giano and Giannandrea, 2014) ultimately separated the Sant'Arcangelo wedge-top basin from the Bradanic foredeep, leading to a change from marine to lacustrine deposition in the basin from 1.0–0.7 Ma (Zavala, 2000; Mattei et al., 2004; Sabato et al., 2005; Capalbo et al., 2010). Subsequently, the Pliocene to Pleistocene Sant'Arcangelo wedge-top basin units were uplifted along with the Nocara ridge in response to progressive post-orogenic (<0.7 Ma) southern Apennines uplift to the southeast (e.g., Cinque et al., 1993; Amato and Cinque, 1999; Ascione et al., 2012). Thin-skinned denudation (Schiattarella et al., 2006; Mazzoli et al., 2008) was generated in response to upper crustal collapse and is believed to have occurred contemporaneously with the compressional deformation of the Apulian Platform carbonates at depth (e.g., Cello and Mazzoli, 1998; Shiner et al., 2004; Mazzoli et al., 2014). At around 0.7 Ma (e.g. Patacca and Scandone, 2001), the southern Apennines were dominated by extension along high-angle normal faults (e.g., Cello et al., 1982; Cinque et al., 1993; Hippolyte et al., 1994; Ascione and Cinque, 1999) that is believed to have overprinted the entire tectonic sequence at depth as well as in the near surface, cutting across the low-angle extensional faults in the upper crust (Mazzoli et al., 2014). Coeval with the onset of extensional deformation, the northeastern side of the southern Apennines experienced uplift starting in the Middle Pleistocene, which is believed to be due to the slab detachment and rebound of the Apulia lithosphere (e.g., Cinque et al., 1993; Ascione et al., 2012, and references therein). Middle to late Pleistocene marine terraces from the Ionian coastal belt point to post-orogenic uplift increasing from NE to SW (e.g., Bordoni and Valensise, 1999; Amato, 2000).

3. Study area

3.1. High topography architecture and development

The topographic framework of the western part of the Mt. Alpi region is defined by high isolated carbonate peaks and ridges (elevations >1600 m) bound by well-developed semi-elongate to elongate intermontane basins (Fig. 1a). The high topography along the western chain axis primarily consists of Apennine Platform carbonates (e.g. Mts. Raparo, La Spina and Pollino), while Mts. Alpi and Sirino are made up of Apulian Platform and Lagonegro carbonates, respectively, that are typically found structurally lower in other locations of the southern Apennines (Fig. 2) (Mazzoli et al., 2001; Aldega et al., 2003; Corrado et al., 2005). The morphology of these high peaks is typically defined by steep peaks >30° and distinct high-angle normal faults (Mazzoli et al., 2014), reflective of the most recent thick-skinned extension. This is especially evident at Mt. Alpi, where a steep (~50°) high-angle fault scarp controls the morphology of the western flank of the mountain (Fig. 3a) (Mazzoli et al., 2014). Three of these high peaks (Mts. Sirino, La Spina and Pollino) extend along the southern Apennines drainage divide trending ~NW-SE with the chain axis, while two isolated peaks (Mts. Alpi and Raparo) located east of the drainage divide follow a ~N-S trend and stand above the surrounding topography despite being located away from the drainage divide and line of maximum elevation (Fig. 1a). Topographic profiles both along and across the chain axis reveal a locus of high topography between Mts. Sirino, Alpi, La Spina and Raparo peaks, with elevation decreasing progressively to the east and west but dropping more sharply north of Mt. Raparo, south of Mt. Alpi and west and south of Mt. Sirino (Fig. 1b). The Cogliandrino River valley extending ~N-S between Mts. Sirino and Alpi also stands notably higher than surrounding basins as part of the local topographic high.

Complementing the topographic evidence for surface uplift, low-temperature thermochronometry data from bedrock samples show that the pattern of recent exhumation also coincides with the local topographic high. Young apatite (U–Th)/He (AHe) and fission track (AFT) cooling ages (ranging from 1.6 to 1.9 Ma and 1.5 to 3.2 Ma, respectively) from Mt. Alpi and Mt. Sirino (Corrado et al., 2005; Mazzoli et al., 2006, 2008, 2014; Iannace et al., 2007; Invernizzi et al., 2008), located in the footwall of the ~ESE-vergent Cogliandrino low-angle detachment fault, reflect rapid exhumation (~1 mm/yr) of these units, with rates decreasing to <0.6 mm/yr starti'ng at ~1.5 Ma (Fig. 1) (Mazzoli et al., 2014). Bedrock cooling ages north and south of the Mt. Alpi area are notably older than those from Mts. Alpi and Sirino (AHe = 3.4 to 5.9 Ma and AFT = 3.8 to 9.2 Ma), with exhumation rates inferred to be <0.6 mm/yr from at least 4 Ma to the Present (Mazzoli et al., 2014). Despite the close proximity of Mt. Raparo to Mts. Alpi and Sirino, this peak is believed to have experienced a different exhumation history because it is located in the hanging wall of the Cogliandrino detachment fault (Mazzoli et al., 2014).

3.2. Intermontane basins

The intermontane basins interspersed between the high carbonate peaks collectively formed in response to ~NE-SW Quaternary extension

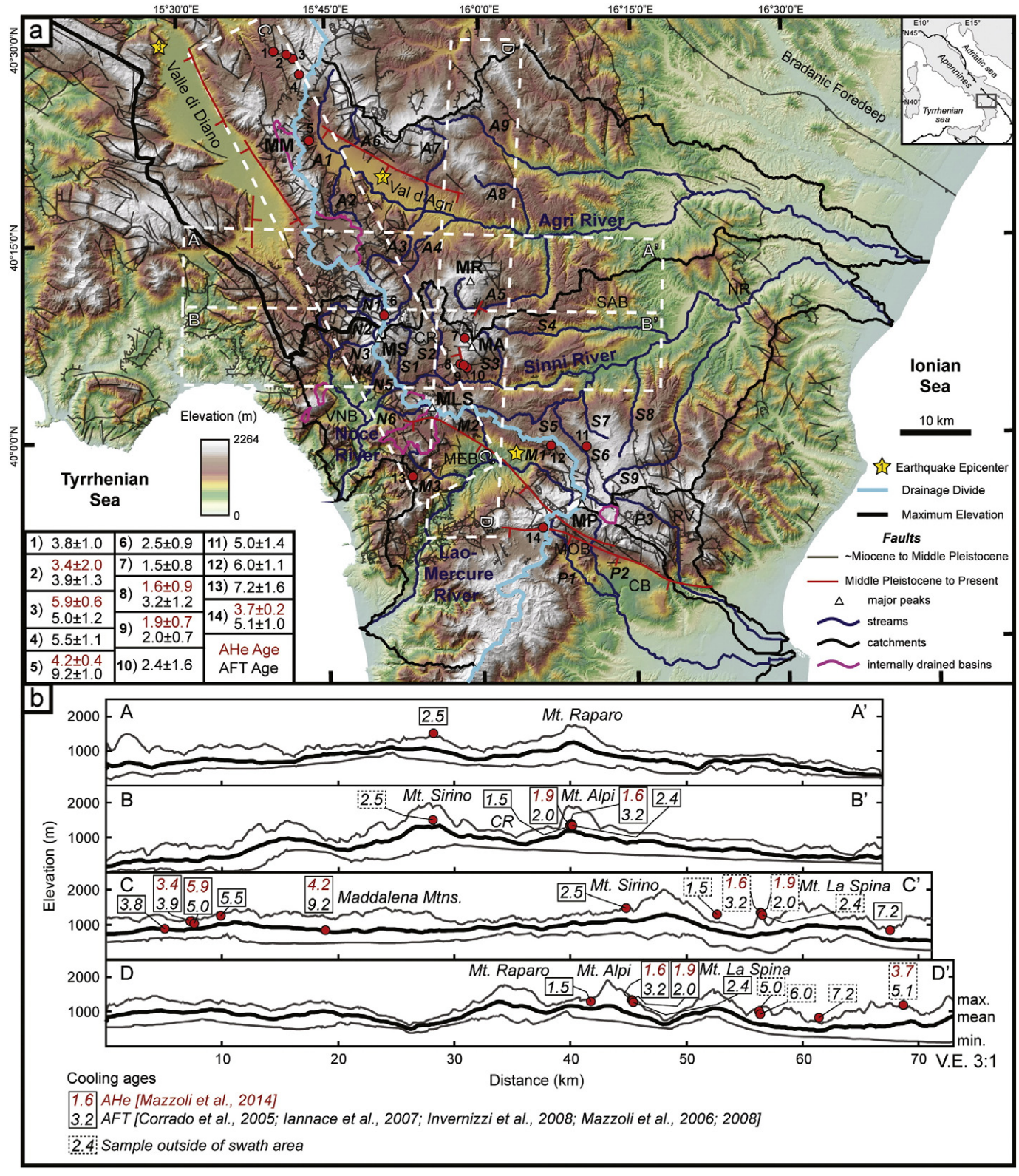

Fig. 1. (a) Shaded relief map of the Mt. Alpi region created in ArcGIS using 10 m digital elevation model (DEM) data from the Istituto Nazionale di Geofisica e Vulcanologia (INGV) (Tarquini et al., 2007, 2012), showing streams analyzed in this study. Stream numbers on map correspond to respective stream profiles in Fig. 4. Fault data modified from Bonardi et al. (1988) and Papanikolaou and Roberts (2007). Stars represent measured (1) and estimated (2, 3) epicenter locations for past earthquakes: 1 = M_w 5.6 Lauria earthquake in 1998, 2 = M_w 7.0 Val d'Agri earthquake in 1857 and 3 = M_w 6.4 Vallo di Diano earthquake in 1561. Figure modified from Buscher et al. (2015). Parameters chosen for shaded relief map based on suggestions at gis4geomorphology.com (b) Elevation swath profiles trending roughly perpendicular (AA' & BB') and parallel (CC' & DD') to the chain axis and primary tectonic structures. Swath profiles figure modified from Mazzoli et al. (2014). Abbreviations: MA = Mt. Alpi, MS = Mt. Sirino, MR = Mt. Raparo, MLS = Mt. La Spina, MP = Mt. Pollino, MM = Maddalena Mountains, VNB = Valle del Noce Basin, MEB = Mercure Basin; MOB = Morano Basin, CB = Castrovillari Basin, RV = Raganello Valley, CR = Cogliandrino River, SAB = Sant'Arcangelo Basin, NR = Nocara Ridge, V.E. = vertical exaggeration, numbers 1–14 correspond to low-temperature thermochronometry data in table.

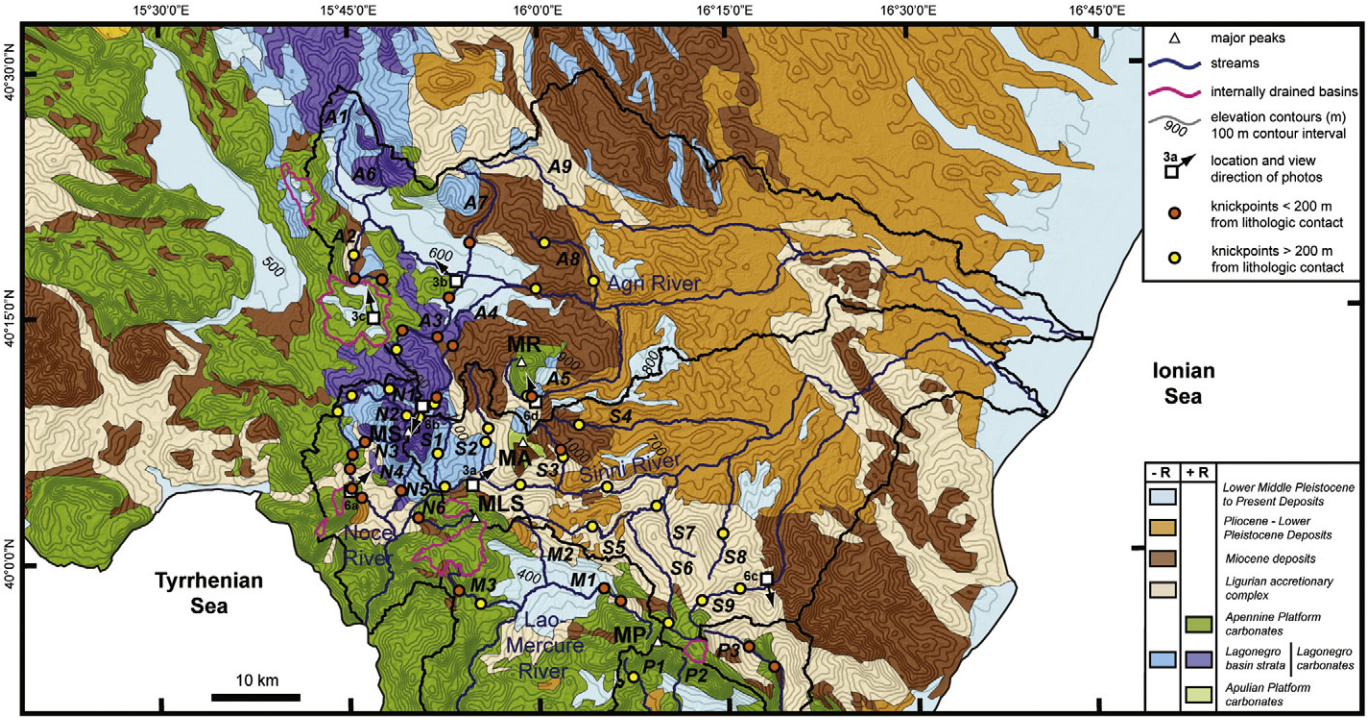

Fig. 2. Lithologic map of the Mt. Alpi area. Geologic data compiled and modified from Bonardi et al. (1988), Ascione et al. (2012) and Mazzoli et al. (2012). Lithologic units are broadly classified as either more (+R) or less (−R) resistant to weathering. Contours generated in ArcGIS using 10 m DEM data from the INGV (Tarquini et al., 2007, 2012). Contour interval = 100 m.
Modified from Buscher et al. (2015). Photo location symbols include figure number (e.g. 3a is Fig. 3a).

documented throughout the region and each reflect a distinct stage of extension (Figs. 1a and 3b) (e.g., Cello et al., 1982; Hippolyte et al., 1994; Montone et al., 1999; Frepoli and Amato, 2000; Caiazzo et al., 2006; Ascione et al., 2007, 2013; Spina et al., 2008; Devoti et al., 2011; Pierdominici and Heidbach, 2012; Faure Walker et al., 2012; Candela et al., 2015). The Vallo di Diano located west of the Agri catchment is a well formed elongate ~NNW-SSE-oriented half-graben (e.g., Santangelo, 1991; Ascione et al., 1992; Cello et al., 2003; Barchi et al., 2007; Amicucci et al., 2008), bound to the northeast by a relatively linear mountain front formed by three high-angle normal fault segments that are believed to have been active from the early Pleistocene to the Present (Cello et al., 2003; Galli et al., 2006; Papanikolaou and Roberts, 2007; Spina et al., 2008; Villani and Pierdominici, 2010).

Roughly aligned with the Vallo di Diano is the notably smaller and less developed Valle del Noce basin, which hosts a deeply eroded and dissected lacustrine succession from the late part of the Early Pleistocene to the early Middle Pleistocene (La Rocca and Santangelo, 1991). A faceted scarp on the northeastern side of the Noce valley suggests that formation of the Noce basin could be related to a fault trending ~NW-SE (Valente, 2009). Basin formation likely followed the development of the Vallo di Diano, causing streams originally flowing northward to reverse course (I.S.P.R.A., in press).

Southeast of the Noce valley lies the Mercure basin, an equidimensional extensional lacustrine basin believed to have been active from the early part of the middle Pleistocene (Schiattarella, 1998; Schiattarella et al., 2003, 2006; Capalbo et al., 2010; Robustelli et al., 2014), which is framed on the northeast by a high-angle fault system trending ~WNW-ESE. The Mercure basin is thought to have formed with the Morano and Castrovillari basins in the hanging wall of the Pollino fault system, which initiated as a sinistral fault in the lower Pleistocene and ultimately became a normal fault system in the middle Pleistocene, with extension directed ~NE-SW (Schiattarella, 1998; Robustelli et al., 2014). Cessation of activity of the Mercure lacustrine basin at ~500 ka (Petrosino et al., 2014; Robustelli et al., 2014) and the Noce basin occurred from the progressive incision of rivers flowing towards the Tyrrhenian Sea, triggered by down-faulting and associated eastward coastline migration generated in response to the extension of the Tyrrhenian back-arc basin (e.g., La Rocca and Santangelo, 1991; Robustelli et al., 2014). Based on ages from marine terrace deposits (Filocamo et al., 2009, 2010), the present-day Tyrrhenian coastline was established at around the beginning of the middle Pleistocene.

The Val d'Agri in the upper reach of the Agri catchment is a well-developed elongate intermontane basin (Fig. 3b) considered to be relatively nascent based on the presence of two isolated depocenters (Morandi and Ceragioli, 2002; Colella et al., 2004) and segmented Quaternary faults (Cowie et al., 2000; Cowie and Roberts, 2001). However, extensional faulting along the Val d'Agri basin dates back to the Middle Pleistocene (e.g., Di Niro et al., 1992; Boenzi et al., 2004) and has been documented only until 40–20 ka (Giano et al., 2000; Candela et al., 2015).

In addition to sedimentary basins, numerous polje (basins formed by karstic processes) are found at catchment boundaries, especially along the main drainage divide (Figs. 1a and 3c). Features like these are quite ubiquitous throughout the Apennines, with polje basins and tufa and travertine deposits being typically found close to large normal faults (e.g., Minissale, 2004; Santo et al., 2011; Brogi et al., 2012; Ascione et al., 2014). The formation of these features near active faults is believed to be related to the transfer of CO_2-rich fluids along fault zones that leads to precipitation of the fluid at the surface (e.g., Kerrich, 1986; Toutain and Baubron, 1999; Sibson, 2000; Cello et al., 2001; Ciotoli et al., 2007; Ascione et al., 2014).

3.3. Seismicity

The high-angle normal faults that define many of the steep mountain fronts in the southern Apennines have also been the sources of significant historical earthquakes (Fig. 1a). Seismic data interpretations and the distribution of surface perturbations from the Mw 5.6 Lauria earthquake in 1998 showed that the rupture was triggered along a northwest-trending fault at the northwestern end of the Mercure

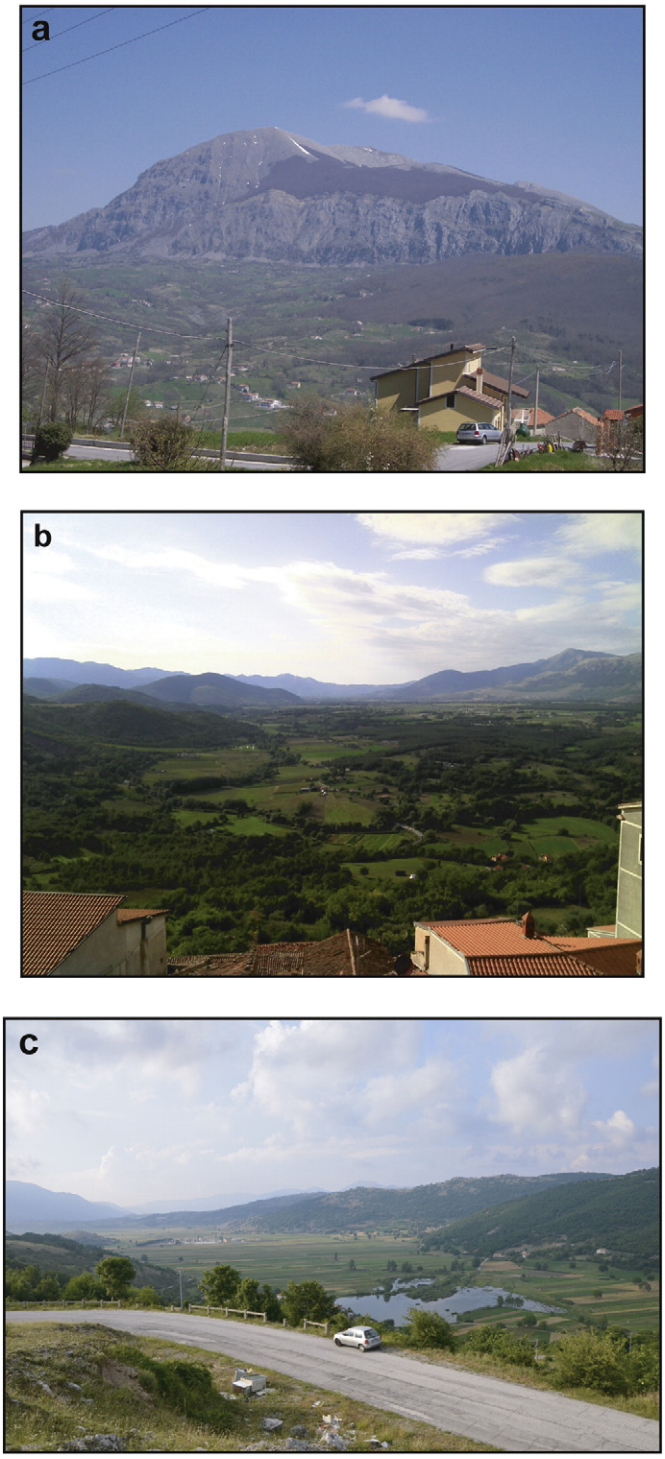

Fig. 3. (a) Looking ~NE at Mt. Alpi and Cogliandrino valley. (b) Looking ~NW at Val d'Agri. (c) Looking ~N at SE end of Magorno polje valley. See Fig. 2 for photo locations.

fault, as part of the Pollino fault system (Michetti et al., 2000), or alternatively along a transverse shear zone (Galli et al., 2001). In 1857, the Val d'Agri experienced a Mw 7.0 earthquake (Rovida et al., 2011-CPTI11) believed to be attributed to structures trending NW-SE that frame the Val d'Agri to the northeast (Fig. 1a) (Pantosti and Valensise, 1988; Benedetti et al., 1998; Borraccini et al., 2002; Michetti et al., 2000). Relatively close to the Val d'Agri epicenter, a Mw 6.4 earthquake occurred in 1561 near the northern end of Vallo di Diano (Working Group CPTI, 2004). This correlation between earthquake data and mountain peak morphology suggests high-angle faults common to the Mt. Alpi region connect to deeper structures and exhibit late Quaternary activity (e.g., Michetti et al., 2000; Macchiavelli et al., 2012), illustrating that surface features may reflect recent extension (Mazzoli et al., 2014).

4. Methods

To help document the landscape development of the Mt. Alpi area, individual tributary and trunk stream profiles from the Agri, Sinni, Noce, Mercure and Pollino catchments were analyzed and compared with features exhibited by the topographic framework of the region (Pollino catchments = Morano and Castrovillari basins and Raganello valley adjacent to Mt. Pollino). Stream profiles were created from each catchment to show 1st-order variations in concavity and convexity along the stream path from source to sink (Fig. 4). Stream profile inflections observed in the field and/or by remote sensing (e.g., DEMs, Google Earth) and not associated with human-made structures were classified as knickpoints and labelled on the lithologic map (Fig. 2).

To provide quantitative constraints on the geometric framework of the region, stream profiles were analyzed using four different approaches: (1) stream length-gradient (SLG), (2) normalized channel steepness (k_{sn}) (3) stream convexity and (4) first-order channel gradient indices (Hack, 1957; Flint, 1974; Merritts and Vincent, 1989; Demoulin, 1998; Snyder et al., 2000; Zaprowski et al., 2005; Spagnolo and Pazzaglia, 2005; Wobus et al., 2006). The SLG, k_{sn} and stream convexity analyses were conducted using 10 m digital elevation model (DEM) data obtained from the INGV (Tarquini et al., 2007, 2012) and the first-order channel gradient analyses utilized 90 m SRTM data (NASA).

The SLG index quantifies stream profile steepness at the reach scale by multiplying the ratio of the local slope ($\Delta H/\Delta L$) centered around a midpoint of a given reach by the stream length (L) measured from the headwaters to the reach midpoint (Fig. 5a) ($S = (\Delta H/\Delta L)^*L$; Hack, 1957). This approach is typically used to distinguish variations in stream gradient generated by changes from such factors as tectonic uplift, rock type, or surface processes. In this study, the SLG index values were determined by measuring the change in stream length and height between 25 m contours generated in ArcGIS for the 10 m DEM and multiplied by the upstream length from the midpoint of the stream reach between contours. The 25 m contour interval was chosen to be consistent with the original 25 m topographic map contour interval used to create the 10 m DEM data (Tarquini et al., 2007) and to help reduce the amount of extraneous data that may be inadvertently introduced during the process of converting the cartographic data to digital form (e.g., Wobus et al., 2006).

The k_{sn} index expands on the fundamentals of the SLG index by comparing the reach slope (S) with the catchment area (A) upstream of the reach midpoint to the power of the concavity index (Θ) to ultimately obtain the channel steepness index k_s (Fig. 5a) ($S = k_s A^{-\Theta}$; Hack, 1957, Flint, 1974, Snyder et al., 2000, Wobus et al., 2006; Kirby and Whipple, 2012). Because slight deviations of the concavity index (slope of the gradient-area data) can produce a wide range of values of channel steepness index (y-intercept of the slope) when comparing streams from catchments varying in size, the data need to be normalized using a reference concavity (Θ_{ref}) calculated from the error-weighted mean concavity of the streams analyzed (Wobus et al., 2006; Kirby and Whipple, 2012). For the Mt. Alpi area, the normalized steepness index (k_{sn}) was determined following the automated k_{sn} procedure of the stream profile tool created by Whipple et al. (2007) and found at www.geomorphtools.org, using the following parameters: $\Theta_{ref} = -0.48$, smoothing window = 250 m, sampling interval = 25 m, minimum catchment size = 10^8 m^2. The Θ_{ref} of −0.48 represents the error-weighted mean concavity determined from the best-fit slope of select gradient-area data (Snyder et al., 2000; Wobus et al., 2006) from each of the 30 streams analyzed in this study (see Appendix). The smoothing window size was chosen based on suggestions by Whipple et al. (2007) to use 250 m for USGS DEMs, which have a similar resolution to those downloaded from the INGV. The 25 m contour interval was selected to be consistent with the SLG index analyses and the

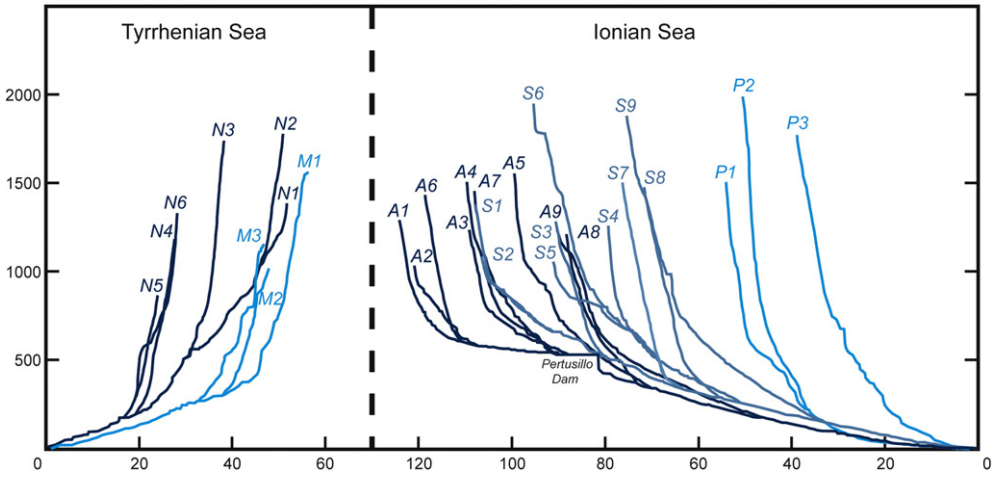

Fig. 4. Stream profiles extracted in ArcGIS from 10 m DEM data obtained from INGV (Tarquini et al., 2007, 2012), showing difference in steepness, length, and general character between streams from the Tyrrhenian and Ionian catchments.

minimum catchment size of 10^8 m^2 was chosen to allow for analyses of the same stream lengths as by the other techniques in the study and to reduce the potential for clutter from a high density of streams. Knickpoints were also identified based on inflections observed along stream profiles and the vertical clustering of points on gradient-area plots generated from the stream profile tool (Whipple et al., 2007).

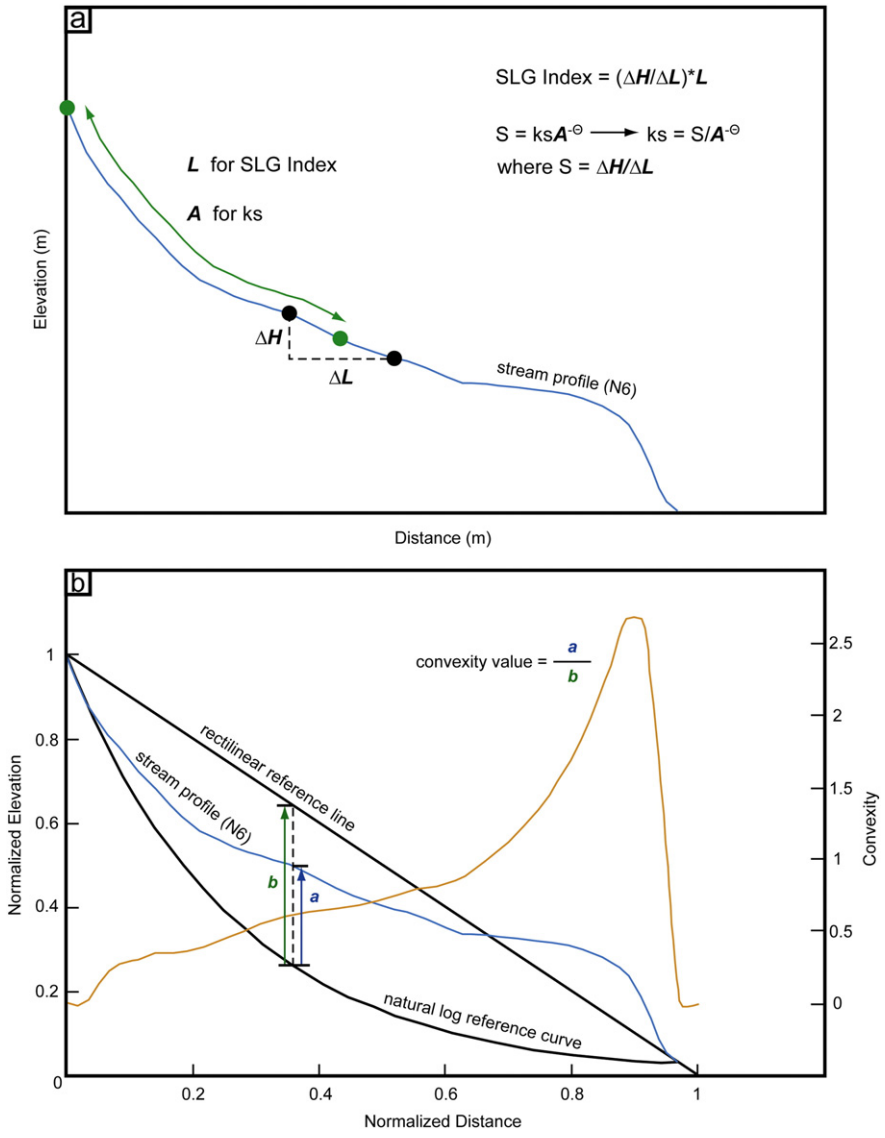

Fig. 5. Diagrams illustrating measurement and calculation of (a) stream length-gradient and channel steepness indices and (b) stream convexity. See Methods section for details.

The method for quantifying stream convexity, representing an extension of methodologies applied by Demoulin (1998) and Zaprowski et al. (2005), compares the original DEM stream profile with two normalized reference profiles: one represented by a natural log curve plotted between the upstream and downstream endpoints (high concavity end-member), and a second rectilinear curve plotted through these same points (high convexity end-member) (Fig. 5b). Unlike the methods of Demoulin (1998) and Zaprowski et al. (2005) that inferred the stream concavity index from the ratio of observed incision with maximum incision, the measurement of stream convexity compares the difference between the DEM stream profile and theoretical steady-state profile represented by the natural log curve (observed convexity) with that between the rectilinear and natural log curves ('maximum' convexity). Therefore, the higher the DEM profile-natural log values relative to the rectilinear-natural log values, the higher the stream convexity. These ratios can become more variable closer to the upstream and downstream ends of the profiles due to the convergence of the three curves, but these variations are not considered problematic since recent uplift changes are best expressed in the middle reaches of bedrock-floored rivers, not masked by hillslope and alluvium processes observed in upper and lower river reaches, respectively (e.g., Sklar and Dietrich, 1998; Montgomery and Foufoula-Georgiou, 1993; Whipple and Tucker, 2002; Stock and Dietrich, 2003). Sample spacing was set at 250 m to be consistent with the smoothing window size used for the stream profile tool for the gradient-area analyses (Whipple et al., 2007) and to help reduce data noise.

In addition to stream profile analyses of high-order trunk and tributary rivers, first-order channel gradient analyses were conducted on Pliocene to Pleistocene Sant'Arcangelo basin units. The comparatively low energy setting of low-order rivers allows for longer preservation of slope perturbations (Merritts and Vincent, 1989; Spagnolo and Pazzaglia, 2005), thereby making first-order channel analyses a good proxy for quantifying differential uplift. Because lithology can be a primary control on the profiles of first-order streams, analyses were only applied to the Sant'Arcangelo basin units representing the largest homogeneous rock unit in the field area, which extend across both the Agri and Sinni catchments. First-order channel gradient analyses were calculated using 90 m SRTM data (NASA).

5. Results

Stream profiles from the study area show that profile steepness and convexity are generally higher in the Noce and Mercure catchments followed by medium values in the Sinni and Pollino catchments and low values in the Agri catchment, while stream lengths are greatest in the Agri and shortest in the Noce (Fig. 4). The steep short reaches along the western flank of Mt. Sirino in the Noce catchment form a distinct radial pattern compared to the longer less steep reaches east of the peak (Figs. 1a, 4, 6a, and b). In contrast, streams surrounding the Pollino massif from the Mercure catchment and upper reaches of the Pollino and Sinni catchments are all characterized as steep (Figs. 4 and 6c).

Numerous knickpoints, found primarily in the western part of the field area, can be categorized into two groups based on the apparent correlation, or lack thereof, between lithology and knickpoint location (Fig. 2). The first group consists of knickpoints in the Noce, Mercure and Pollino catchments and along tributaries leading to the Val d'Agri that are located within 200 m of lithologic contacts. The second group is found primarily in the more erodible rocks of the central part of the study area along Mts. Alpi and Raparo and the northern flank of Mt. Pollino with no obvious influence from lithology (i.e. >200 m away from the nearest lithologic contact).

For the quantitative profile analyses, the SLG, k_{sn} and stream convexity data generally exhibit a similar distribution of high and low values relative to the high topography of the chain axis and lithology but also show localized deviations unrelated to these factors. The SLG index data for the Agri and Sinni catchments increases eastward as rock type transitions from carbonates to conglomerates, with low values in the western upper reaches and medium to high values in the middle reaches to the east (Fig. 7a). The relatively abrupt transition from low to medium-high values occurs along a ~N-S trend that roughly coincides with the alignment of Mts. Alpi and Raparo. The lowest values of the dataset are found along the Agri and Cogliandrino River valleys, while the highest values are along the northern flank of Mt. Pollino, with lithology being surprisingly more erosive in all of these localities relative to other areas with moderate values. SLG index values vary in the Noce catchment but are primarily medium to high at locations along middle reaches that coincide with lithologic changes from resistant carbonates (Lagonegro/Apennine Platform carbonates) to more easily erodible rock (Lagonegro basin strata/Ligurian accretionary complex units). The Mercure and Pollino catchments exhibit a mixed distribution of SLG index values, with the highest values found along the upper reaches of streams originating from Mt. Pollino.

The map of k_{sn} index data displays values generated by the automated k_{sn} application of the stream profile tool (Whipple et al., 2007) for tributaries and trunk streams from catchments with areas $>10^8$ m^2 (Fig. 7b). Since streams were analyzed based on a minimum catchment area of 10^8 m^2 and were not individually selected, significantly more streams were generated by the k_{sn} index procedure than by the other methods used in this study. Analyses from the stream profile tool are based on calculations for bedrock-substrate rivers (Snyder et al., 2000; Kirby and Whipple, 2001, 2012; Wobus et al., 2006), so values from reaches where hillslope and alluvial processes are expected to dominate (typically upper and lower reaches, respectively) are shown for reference but are not considered for interpretation (Sklar and Dietrich, 1998; Montgomery and Foufoula-Georgiou, 1993; Whipple and Tucker, 2002; Stock and Dietrich, 2003).

A map of the k_{sn} values reveals an ~E-W gradient in the Agri catchment and northern part of the Sinni catchment, with low to medium k_{sn} values in the upper and lower reaches of the catchments and medium to high values in the middle reaches (Fig. 7b). An approximately 5 km wide band of high k_{sn} values in the middle reaches of the Agri and Sinni catchments extends adjacent and subparallel to the ~N-S swath of high topography that includes Mts. Alpi and Raparo. For the southern part of the Sinni catchment, high k_{sn} values are found along the northern flank of Mt. Pollino. The Noce catchment exhibits a mix of medium to high k_{sn} values, with high values located primarily at the contacts between erosionally resistant carbonates and detrital rock units as was observed from the SLG index data. The Mercure and Pollino catchments have primarily high k_{sn} values at the boundary with the Agri catchment, especially along the flanks of Mt. Pollino.

For the stream convexity analyses, the Agri and Sinni catchments generally exhibit an ~E-W change comparable to the previous analyses, with relatively low convexity values in the upper and lower reaches and medium to high values centered along the high topography of Mt. Alpi and Mt. Raparo (Fig. 7c). However, some streams from the Agri and Sinni catchments are in stark contrast to the stream gradient data, with high convexity values found along reaches that have low SLG and k_{sn} index values (e.g., A2, S2, S5), which is especially evident when compared to k_{sn} averages calculated for bedrock reaches (Fig. 7d). Interestingly, the upper reaches of streams M1 and P1 show the opposite trend, with high overall SLG and k_{sn} index values but low convexity values. In the Noce catchment, high convexity values are most common in the upper reaches while high k_{sn} values are more confined to the middle reaches (N1, N4, N5, N6). The same relationship is also observed along other reaches (A5, A9, S3, S6), where the high convexity values are found just upstream of the high k_{sn} values. This variation in reach location for the same knickzone feature may be explained by the different approaches of the two techniques. The stream convexity approach documents the stream profile deviations from a natural log concave reference curve, so the highest values are likely going to be atop a knickpoint as well as the area immediately upstream of the knickpoint. The k_{sn} index displays stream profile deviations associated with the

downstream component of a knickpoint and therefore appears downstream of some high convexity index zones. However, it should be noted that the k_{sn} index can yield low values for streams that are clearly convex as is the case for streams A2, S2 and S5, so it may be helpful to use both techniques in conjunction.

First-order channel gradient analyses show a distinct increase in value from north to south, with the highest values located at ridges straddling the middle reach of the Sinni River (Fig. 7d). The lowest values are found primarily along ridges north of the Agri River but also at ridges bounding the Agri River. First-order channel values also generally increase to the west-southwest towards Mts. Alpi and Raparo.

6. Discussion

Stream network analyses from catchment to reach scale suggest that incision varies along the drainage boundary. The relatively large, elongate, ~E-W orientated Agri and Sinni catchments east of the primary Apennine drainage divide contrast with the smaller, ~N-S oriented Noce and Mercure catchments to the west and south, respectively, implying that incision may generally differ between Tyrrhenian- and Ionian-directed catchments (Fig. 1). The lack of significant incision of the ~NW-SE oriented Val d'Agri basin compared to the moderately incised ~N-S Cogliandrino valley may reflect a general trend of increased upper-reach incision in the south compared to that in the north (Fig. 1).

The apparent correlation between steep and convex stream profiles and catchment location appears to reflect a distinction between catchments located ~E or ~W of the drainage divide and possibly a more subtle ~N-S gradient between the Agri and Sinni catchments (Fig. 4). This contrast in stream profile steepness and convexity at the drainage divide is exemplified at Mt. Sirino (Figs. 4, 6a, and b), indicating that stream incision may vary along this stretch of the drainage divide, while the consistently steep reaches flanking Mt. Pollino suggest incision is at a relatively more mature stage (Figs. 4 and 6c). The presence of internally drained basins with active polje features along the crest of the drainage divide (Figs. 1 and 3c) generally reflects a lack of stream incision and upper hillslope erosional processes controlling the formation of these polje basins, suggesting that variable factors may influence the formation of the drainage divide. The correlation between karstic features and fault zones found in other areas of the southern Apennines (e.g., Santo et al., 2011; Ascione et al., 2014) suggests that faults may play a role in establishing and/or stabilizing drainage divides for a period of time before incision becomes more dominant. Taken together, these gross topographic and drainage network features appear to indicate that a transient drainage divide exists in the Mt. Alpi region, but more in-depth analyses of stream network patterns at the catchment scale and stream profile surface changes at the reach scale are needed to better constrain the landscape response to localized uplift.

Analyses of bedrock-floored stream reaches in the Agri and Sinni catchments show that high SLG, k_{sn} and stream convexity indices trend ~N-S with Mts. Alpi and Raparo and the northern flank of Mt. Pollino. A swath of high values of SLG and k_{sn} indices in the Agri and Sinni catchments are located immediately east of Mts. Alpi and Raparo that coincides with the ~N-S alignment of the Pietra del Pertusillo and Latronico gorges (e.g., Giano and Giannandrea, 2014), the fault scarp bounding the southern flank of Mt. Raparo and a distinct knickpoint along stream A8 (Figs. 2 and 6d). High stream convexity values are also focused along the same ~N-S trend but follow a wider swath on both sides of Mts. Alpi and Raparo (Fig. 7c). High values of SLG and k_{sn} indices also dominate the upper stream reaches of Mt. Pollino, but surprisingly one of the most convex streams in the entire field area (S5) originates from a lower elevation peak to the northwest of Mt. Pollino

Fig. 6. (a) Looking ~NE at west side of Mt. Sirino with village of Rivello seen in the foreground. (b) Looking ~SW at NE side of Mt. Sirino. (c) Looking ~S at tributary streams along northern flank of Mt. Pollino. (d) Looking ~NW at SE flank of Mt. Raparo, with village of Castelsaraceno seen in middleground. See Fig. 2 for photo locations.

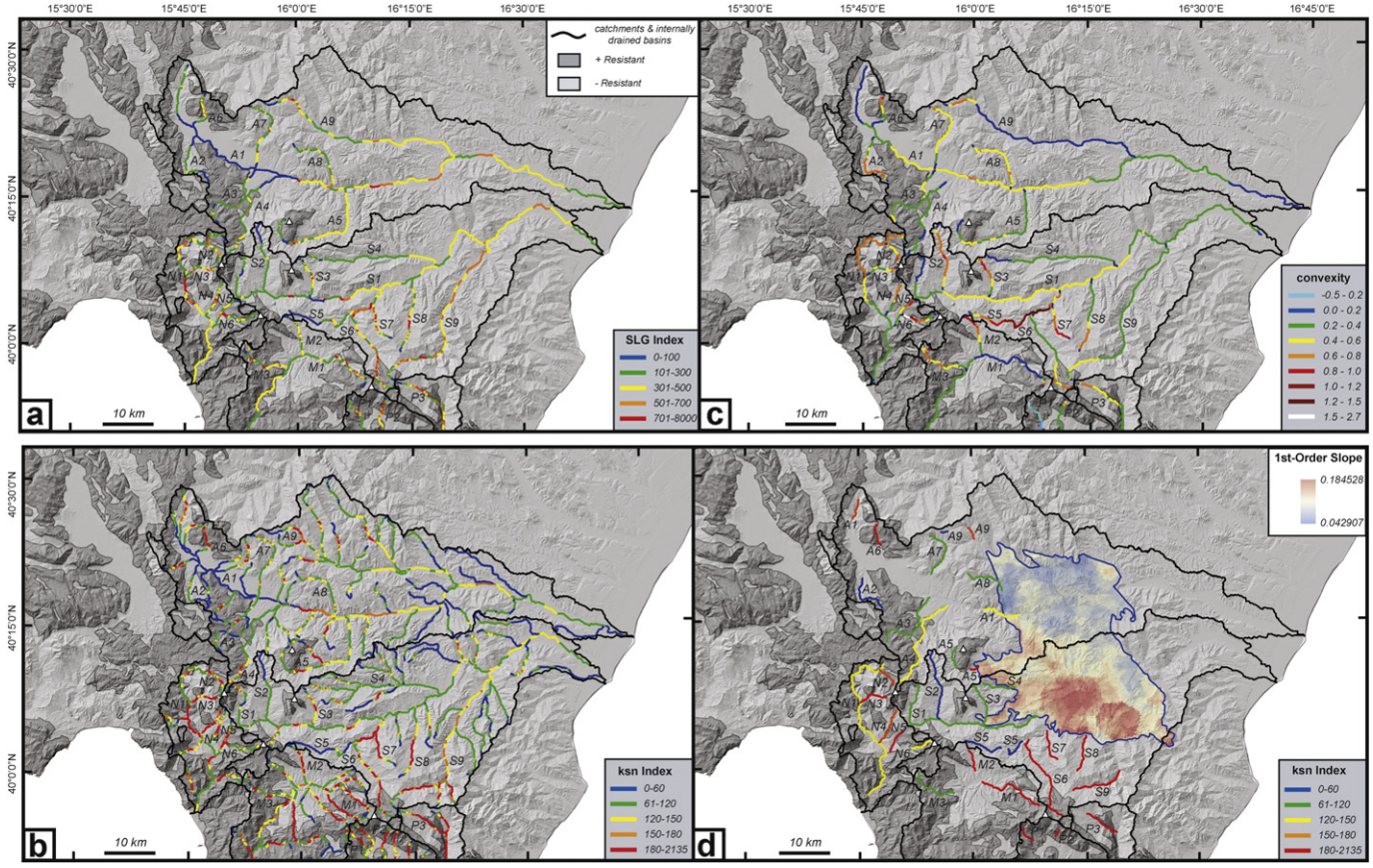

Fig. 7. Map view of (a) stream length-gradient, (b) normalized channel steepness, (c) stream convexity and (d) first-order channel gradient indices data. Normalized channel steepness data were created by stream profiler tool developed by Whipple et al. (2007). Key tributaries were individually selected for stream length-gradient index and stream convexity data while normalized channel steepness index streams were selected based on a watershed threshold (10^8 m^2) that yielded significantly more stream analyses. The area used for the first-order channel gradient analyses follows the mapped Pliocene-Pleistocene Sant'Arcangelo basin unit (Bonardi et al., 1988; Ascione et al., 2012 and Mazzoli et al., 2012). Included in Fig. 7d are the traces of bedrock stream reaches estimated by the distribution of gradient-area data (see Appendix) and remote sensing observations (DEMs, Google Earth). The length of each stream reach in Fig. 7d correlates with the best-fit line shown in the gradient-area plots and the value reflects the average channel steepness index value for each reach analyzed (see Appendix). Stream length-gradient index, normalized channel steepness and convexity analyses were conducted with 10 m DEMs obtained from the Istituto Nazionale di Geofisica e Vulcanologia (INGV) (Tarquini et al., 2007, 2012) and the first-order channel gradient index data was analyzed using 90 m SRTM data.

that flows roughly perpendicular to the ~N-S oriented Pollino and Mercure streams (Fig. 7c). The low k_{sn} but high stream convexity values of this and two other tributary streams analyzed near the drainage divide (A2 and S2) suggest that uplift may have been generated without a notable vertical response detectable by k_{sn} analyses at the local reach level. In contrast, streams originating from Mt. Pollino generally have high values of SLG and k_{sn} indices as well as convex profiles, with the exception of streams M1 and P1 that have considerably lower convexity values, suggesting perturbations along the stream channel may be more localized and not reflective of broad regional uplift as can be interpreted from the distribution of high values between the SLG and k_{sn} indices for these streams.

Fluvial and karstic features west of the Tyrrhenian-Ionian catchment boundary also suggest that the drainage divide is in a transient state. In the Noce catchment, stream analyses along the western flank of Mt. Sirino reveal convex upper reaches and steep (high k_{sn}) middle reaches along the same streams similar to those in the Pollino area, suggesting that the surface expression of uplift may be more localized. This is supported by the presence of hanging stream valleys along the southeastern section of the Noce catchment (e.g., very steep reach of N6). Active polje features in the region may reflect a drainage divide that is currently stable but steep stream reaches located adjacent to these features suggest that stability of the current drainage divide should be short-lived. Wind gaps found at ~800 m a.s.l. that dissect carbonate rocks at the boundary between the Vallo di Diano and Noce catchments lend further support for a transient drainage divide.

The fact that the majority of the Apennines has an out-of-phase alignment between the trend of the highest peaks and the primary drainage divide (e.g., Amato et al., 1995; Salustri Galli et al., 2002) supports the possibility that drainage divide migration is also occurring in the Mt. Alpi region.

Considering the distribution of gross topographic features, knickzones, and high convexities coupled with the known tectonic history of the region, the modern landscape appears to be the expression of concurrent tectonic and geomorphic drivers that trend both along and across the chain axis. The presence of the Val d'Agri (e.g., Cello et al., 1982; Montone et al., 1999; Frepoli and Amato, 2000; Caiazzo et al., 2006; Ascione et al., 2007, 2013; Spina et al., 2008; Devoti et al., 2011; Pierdominici and Heidbach, 2012; Faure Walker et al., 2012; Candela et al., 2015), Vallo di Diano (Ascione et al., 1992; Cello et al., 2003; Galli et al., 2006; Papanikolaou and Roberts, 2007; Spina et al., 2008; Villani and Pierdominici, 2010) and Mercure (Michetti et al., 1997; Papanikolaou and Roberts, 2007) intermontane basins may suggest that upper crustal extension has generally migrated both towards and along the Apennine chain axis. Steep convex streams radiating away from Mt. Sirino in the Noce catchment are found adjacent to streams in the Agri and Sinni catchments with low k_{sn} and stream convexity values, suggesting that stream capture is more likely to occur from west to east towards the area of localized uplift, as has been demonstrated at other localities (e.g., Clark et al., 2004; Willett et al., 2014). For example, the >90° turn of stream S1 in the Sinni catchment adjacent to Noce catchment streams N5 & N6 with steep reaches and hanging

valleys around a small polje feature may possibly be the location for stream capture in the near future (Figs. 1 and 8). Evidence for ~-eastward-driven stream capture in the region is supported by the presence of the Castelluccio and Castronuovo Conglomerates, which are located along the northern rim of Mercure basin east of Mt. La Spina and contain pebbles believed to be sourced from bedrock units to the west, signifying that streams may have flowed to the east in early Middle Pleistocene (Capalbo et al., 2010; Mazzoli et al., 2014). These eastward-flowing rivers were subsequently captured by Mercure Basin extension later in the middle Pleistocene at ~700 ka (Mazzoli et al., 2014; Robustelli et al., 2014). Stream S5 located along the northern rim of the Mercure Basin may represent a remnant of these eastward-flowing streams that became abandoned between the active incision of the Mercure Basin and that of the northern flank of Mt. Pollino. Farther north, stream S2 appears to be in the initial stage of adjustment due to continued ~eastward migration and piracy of the Noce streams and uplift of Mt. Alpi and surroundings, which may ultimately lead to the capture of the Cogliandrino valley and eastward migration of the drainage divide (Fig. 8).

Eastward migration of the main divide has already been proposed for the area north of the Mt. Alpi region, related to the growth of catchments in response to Quaternary block faulting along the Tyrrhenian back-arc basin margin and subsequent capture of westward flowing rivers (Amato et al., 1995). For this scenario, limited surface lowering due to the presence of more resistant rocks along the southwestern part of the mountain chain allowed the topographic crest to remain as an elevated ridge west of the main drainage divide (Amato et al., 1995). In the Mt. Alpi region, topographic observations and analyses and constraints on exhumation inferred from cooling age data all suggest that the Mt. Alpi region has been the locus of significant uplift (Corrado et al., 2005; Mazzoli et al., 2006, 2008, 2014; Iannace et al., 2007; Invernizzi et al., 2008). As a result, uplift of Mt. Alpi and the surroundings have likely kept pace with westward fluvial incision, thus allowing the drainage divide and maximum elevation to overlap.

In addition to ~E-W across-strike activity, topographic and stream features appear to reflect a ~N-S component of differential uplift. First-order channel gradient analyses of the Sant'Arcangelo basin show a distinct southward increase in steepness across the Agri and Sinni catchments extending to the northern flank of Mt. Pollino, with no apparent influence by lithology given that analyses were applied only to the Pliocene to Lower Pleistocene Sant'Arcangelo basin units (Fig. 7d). Mt. Pollino streams with high SLG and k_{sn} indices appear to reflect a southward continuation of this trend, with the presence of steep valleys in more easily erodible substrate (Fig. 6c) supporting higher incision in the south. Analyses of river terraces along the Agri and Sinni Rivers in the Sant'Arcangelo basin show a regional southward increase in block tilting starting at ~400 ka (Giano and Giannandrea, 2014), in line with the block tilting inferred from stream and topographic analyses. The southwestward increase in marine terrace uplift along the Ionian Coast supports the patterns exhibited by the Agri and Sinni River

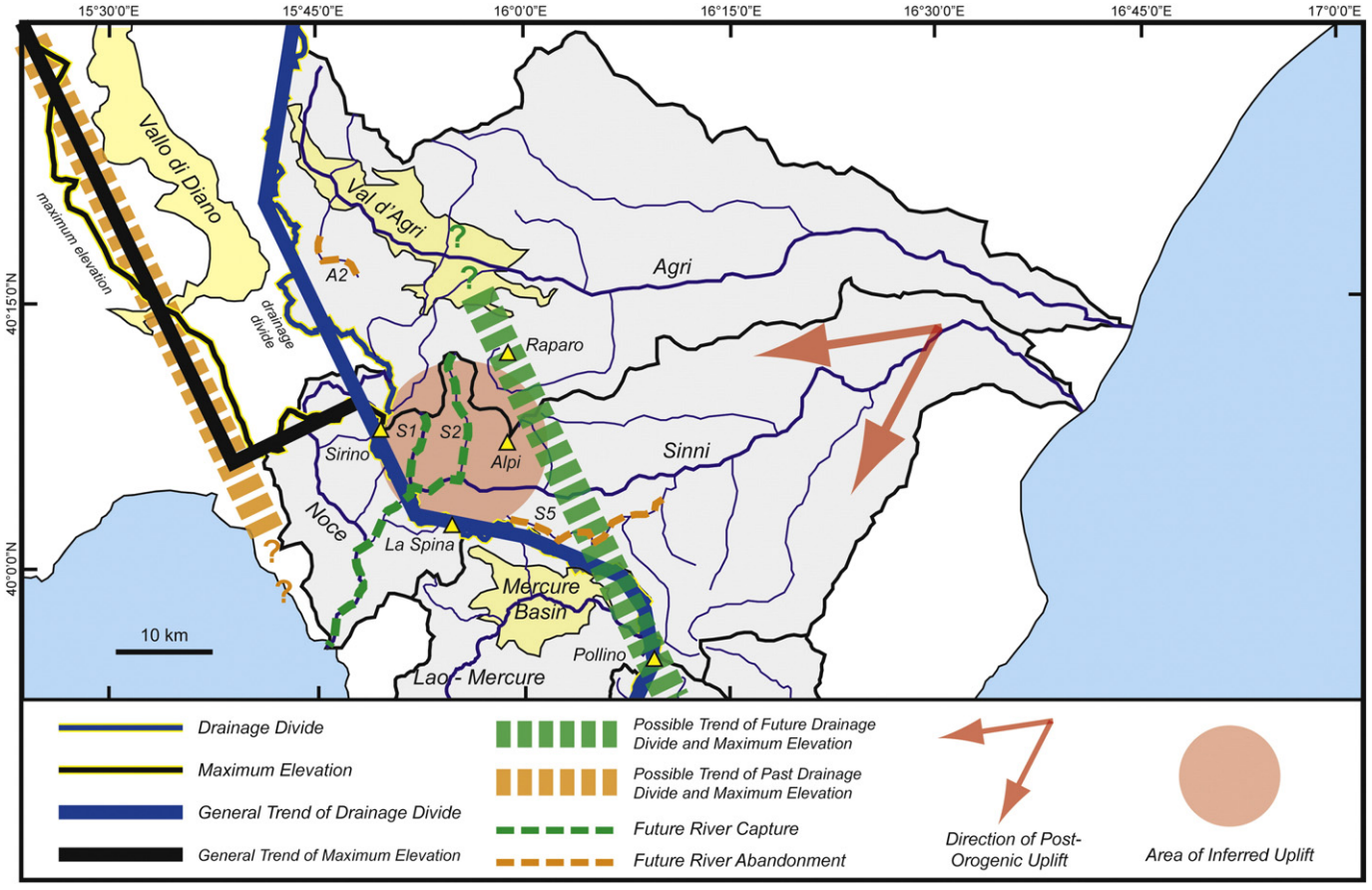

Fig. 8. Schematic diagram illustrating potential past and future scenarios of landscape development in the Mt. Alpi region. Based on the trends of the current drainage divide and maximum elevation (thin blue and black lines with yellow outlines, respectively), topography, cooling age data and stream analyses data, it would appear that exhumation and subsequent surface uplift of Mts. Alpi and Sirino and surroundings (outlined by red circle) may likely lead to river capture of the upper reaches of the Sinni River (S1) and Cogliandrino River (S2) by the Noce catchment (green dashed line). Two streams with high stream convexity but low stream length-gradient and k_{sn} values along the drainage divide (A2 and S5, orange dashed lines) appear to be close to abandonment as a transient stage before the northeastward progression of drainage capture by the Vallo di Diano and Mercure basin, respectively. This restructuring of river geometry may lead to the northeastward migration of the drainage divide and quite possibly the axis of high topography. Red arrows show likely range of directions of increased uplift generated from the tear of the Apulian slab (Ascione et al., 2012 and references therein). See text for details.

terraces and first-order channel analyses. In fact, the trend of increasing uplift inferred by this study is roughly aligned with a region along the Ionian Coast that has recorded a late Pleistocene uplift rate of ~1 mm/yr (Bordoni and Valensise, 1999; Amato, 2000), which may represent an upper limit of recent uplift in the region. However, the lack of anomalies in the core of the Sant'Arcangelo basin and other areas in the east suggest that incision may be keeping pace with relatively slower recent uplift in these areas.

The transient nature of the Mt. Alpi landscape makes the region susceptible to hillslope instability that can be expressed as end-member surface processes such as upper reach incision by debris flows (e.g., Stock and Dietrich, 2003, 2006) or landslides (e.g., Ouimet et al., 2007; Korup et al., 2010). Although these processes can affect stream profiles in the short term, both of these processes are not expected to have played a dominant role in controlling profile anomalies observed in this study. Debris flow incision would be expected to be limited to the steep upper stream reaches (i.e. upper flanks of the high peaks) where hillslopes are less stable and most stream anomalies in the region show no correlation with reach position.

Landslides are pervasive throughout the Mt. Alpi region, but analyses by Santangelo et al. (2013) show that modern-day landslides are primarily reactivated parts of large landslides generated from the Middle Pleistocene to Holocene (Corrado et al., 2002; Schiattarella et al., 2006) that appear to affect only low-order rivers. Considering the dominance of subdued topography in the region (aside from the isolated high peaks), the location of stream profile anomalies irrespective of stream order or reach location, and the systematic increase in first-order gradient indices to the south, it would appear that incision and deposition by mass movements might possibly produce only secondary effects on stream profiles.

7. Conclusions

The modern Mt. Alpi landscape appears to reflect the surface response to tectonically-driven uplift and concurrent basin subsidence as well as erosionally-resistant lithology. The regional cooling age pattern (Corrado et al., 2005; Mazzoli et al., 2006, 2008, 2014; Iannace et al., 2007; Invernizzi et al., 2008) and distribution of elevated topography (Fig. 1) (Mazzoli et al., 2014) reveals a locus of rapid exhumation and subsequent uplift in the Mts. Alpi-Sirino area (Fig. 8). Stream length-gradient (SLG), normalized channel steepness (k_{sn}) and stream convexity indices from the Agri and Sinni catchments show an abrupt ~west-to-east change in value occurring at a ~N-S trend following the alignment of Mts. Alpi and Raparo and a general increase in values to the southeast along the drainage divide (Fig. 7) with no apparent influence from lithology. The Noce catchment to the west has high values occurring at rock unit contacts in numerous locations, suggesting lithology may be a contributing factor for these profile anomalies. Three streams near the drainage divide in the Agri and Sinni catchments exhibit high convexity values despite having low SLG and k_{sn} indices values, suggesting that these streams may be close to abandonment (A2, S5) or capture (S2) due to the northeastward drive of basin subsidence and incision (Fig. 8). The presence of a distinct hanging valley in the Noce catchment (N6) adjacent to a polje feature also suggests that the current drainage divide is unstable.

Considering topographic variations at the orogen scale and stream disturbances at the reach scale, there appears to be evidence for a systematic and possibly trackable landscape expression of tectonic extension (basin subsidence and uplift) and erosionally-resistant lithology that have worked together to maintain both a swath of elevated topography and a separate drainage divide. The most expressive landscape features of extension in the region are the extensional basins, which have acted to force migration of the drainage divides (Amato et al., 1995), sometimes away from the chain of high topography, by creating localized base levels that have trapped and ultimately redirected eastward flowing rivers to the west. The presence of Vallo di Diano between a swath of maximum elevation and the drainage divide would appear to reflect this scenario, while the apparent step in the overlapping maximum elevation-drainage divide lines bounding the Mercure basin may represent a jump of both trends to the northeast due to the uplift of Mt. Pollino, the highest peak in the southern Apennines (Fig. 8).

Surface uplift of the Mts. Alpi-Sirino area likely forced a reconfiguration of the river network at a certain point, with Mt. Sirino acting as the primary headwater source for surrounding streams. Mt. Sirino represents the only junction point for the three primary catchments analyzed in the study area, a characteristic that may reflect relative peak stability as has been shown for major peaks across the globe (Spotila, 2012). In the near future, it is conceivable that the current locus of uplift at Mts. Alpi and Sirino may shift ~eastward based on the notably sharper range front and similar elevation of Mt. Alpi relative to Mt. Sirino. The rivers currently located between Mts. Alpi and Sirino (S1 and S2) may be captured by Noce catchment rivers (e.g., N5) when incision starts to outpace uplift of Mt. Alpi, thereby forcing a drainage divide jump to the northeast (Fig. 8). The progression of northeast-driven basin subsidence and accompanying block uplift along with subsequent drainage divide migration may continue north of Mts. Alpi and Sirino. Concurrent with extension and drainage divide migration in the western part of the study area, the more subdued and easily erodible topography in the east has recently experienced moderate uplift progressing to the southwest subparallel to the Ionian coast (Bordoni and Valensise, 1999; Amato, 2000), likely due to the tear of the Apulia slab (e.g., Cinque et al., 1993; Ascione et al., 2012 and references therein), adding another contributing factor to the uplift pattern of the southern Apennines.

Acknowledgements

The authors would like to thank the editor, Markus Stoffel, and two anonymous reviewers for constructive comments and thoughtful suggestions, Stefano Mazzoli for discussions on the study area during the early stages of the manuscript and Claudia Cannatelli for assistance in the field.

Appendix

Stream profile (top), drainage area vs. distance (middle) and gradient-area (bottom) figures are shown for the 30 streams analyzed in this study. In the stream profile figures, blue crosses along stream profiles represent knickpoints and the blue lines correlate with the best-fit lines in the gradient-area plots. Some pairs of blue crosses represent the starting and ending points of convexities (A9, S2, N5, and M1) and some knickpoints were not shown in Fig. 2 because the locations were away from the bedrock reaches. In the gradient-area plots, blue circles represent knickpoints that correlate with the blue crosses in the stream profile figures and the blue lines represent the best-fit lines through the gradient-area data for the bedrock reaches of the streams. These blue lines from both the stream profile and gradient-area figures are shown in map view in Fig. 7d. The calculated Θ and k_{sn} values for the best-fit lines are also shown in the plots. Labels in gradient-area plots correlate with those in the maps except for the following: acat = a1, ncat = n1, scat = s1, c1 = p1, c2 = p2, d1 = p3.

References

Aldega, L., Cello, G., Corrado, S., Cuadros, J., Di Leo, P., Giampaolo, C., Invernizzi, C., Martino, C., Mazzoli, S., Schiattarella, M., Zattin, M., Zuffa, G., 2003. Tectono-sedimentary evolution of the Southern Apennines (Italy): thermal constraints and modeling. Atti Ticinensi di Scienze della Terra 9, 135–140.

Amato, A., 2000. Estimating Pleistocene tectonic uplift rates in the Southeastern Apennines (Italy) from erosional land surfaces and marine terraces. In: Slaymaker, O. (Ed.), Geomorphology, Human Activity and Global Environmental Change. John Wiley and Sons Ltd., New York, pp. 67–87.

Amato, A., Cinque, A., 1999. Erosional landsurfaces of the Campano-Lucano Apennines (S. Italy): genesis, evolution and tectonic implications. Tectonophysics 315, 251–267.

Amato, A., Cinque, A., Santangelo, N., 1995. Il controllo della struttura e della tettonica plio-quaternaria sull'evoluzione del reticolo idrografico dell'Appennino meridionale. Studi Geol. Camerti 2, 23–30.
Amicucci, L., Barchi, M.R., Montone, P., Rubiliani, N., 2008. The Vallo di Diano and Auletta extensional basins in the southern Apennines (Italy): a simple model for a complex setting. Terra Nova 20, 475–482.
Anders, A.M., Roe, G.H., Montgomery, D.R., Hallet, B., 2008. Influence of precipitation phase on the form of mountain ranges. Geology 36, 479–482.
Ascione, A., Cinque, A., 1999. Tectonics and erosion in the long-term relief history of Southern Apennines (Italy). Zeit. Geomorph. Suppl.-Bd. 117, 1–15.
Ascione, A., Cinque, A., Santangelo, N., Tozzi, M., 1992. Il bacino del Vallo di Diano e la tettonica trascorrente Plio-Quaternaria: nuovi vincoli cronologici e cinematica. Studi Geol. Camerti 1, 201–208.
Ascione, A., Caiazzo, C., Cinque, A., 2007. Recent faulting in Southern Apennines (Italy): geomorphic evidence, spatial distribution and implications for rates of activity. Boll. Soc. Geol. Ital. 126, 293–305.
Ascione, A., Ciarcia, S., Di Donato, V., Mazzoli, S., Vitale, S., 2012. The Pliocene-Quaternary wedge-top basins of southern Italy: an expression of propagating lateral slab tear beneath the Apennines. Basin Res. 24, 456–474. http://dx.doi.org/10.1111/j.1365-2117.2011.00534.x.
Ascione, A., Mazzoli, S., Petrosino, P., Valente, E., 2013. A decoupled kinematic model for active normal faults: insights from the 1980, MS = 6.9 Irpinia earthquake, southern Italy. Geol. Soc. Am. Bull. 125, 1239–1259. http://dx.doi.org/10.1130/B30814.1.
Ascione, A., Iannace, A., Imbriale, P., Santangelo, N., Santo, A., 2014. Tufa and travertines of southern Italy: deep-seated, fault-related CO_2 as the key control in precipitation. Terra Nova 26, 1–13.
Attal, M., Cowie, P.A., Whittaker, A.C., Hobley, D., Tucker, G.E., Roberts, G.P., 2011. Testing fluvial erosion models using the transient response of bedrock rivers to tectonic forcing in the Apennines, Italy. J. Geophys. Res. 116, F02005. http://dx.doi.org/10.1029/2010JF001875.
Barchi, M., Amato, A., Cippitelli, G., Merlini, S., Montone, P., 2007. Extensional tectonics and seismicity in the axial zone of the Southern Apennines. Boll. Soc. Geol. Ital. 7, 47–56.
Benedetti, L., Tapponnier, P., King, G.C.P., Piccardi, L., 1998. Surface rupture of the 1857 southern Italian earthquake? Terra Nova 10, 206–210.
Boenzi, F., Capolongo, D., Cecaro, G., D'Andrea, E., Giano, S.I., Lazzari, M., Schiattarella, M., 2004. Evoluzione geomorfologica polifasica e tassi di sollevamento del bordo sud-occidentale dell'alta Val d'Agri (Appennino meridionale). Boll. Soc. Geol. Ital. 123, 357–372.
Bonardi, G., D'Argenio, B., Perrone, V., 1988. Carta geologica dell'Appennino meridionale. Mem. Soc. Geol. Ital. 41, 1341.
Bonnet, S., 2009. Shrinking and splitting of drainage basins in orogenic landscapes from the migration of the main drainage divide. Nat. Geosci. 2, 766–771. http://dx.doi.org/10.1038/ngeo666.
Bordoni, P., Valensise, G., 1999. Deformation of the 125 ka marine terrace in Italy: tectonic implications. Geol. Soc. Lond., Spec. Publ. 146, 71–110.
Borraccini, F., De Donatis, M., Di Bucci, D., Mazzoli, S., 2002. 3D model of the active extensional fault system of the high Agri River valley, southern Apennines, Italy. J. Virtual Explor. 6, 1–6.
Brogi, A., Capezzuoli, E., Buracchi, E., Branca, M., 2012. Tectonic control on travertine and calcareous tufa deposition in a low-temperature geothermal system (Sarteano, Central Italy). J. Geol. Soc. Lond. 169, 461–476.
Buscher, J., Ascione, A., Valente, E., Mazzoli, S., 2015. Inferring surface uplift from longitudinal stream profiles in the Mt. Alpi area, southern Apennines, Italy. Miscellanea INGV. 27, 66–70.
Butler, R.W.H., Mazzoli, S., Corrado, S., De Donatis, M., Di Bucci, D., Gambini, R., Naso, G., Nicolai, C., Scrocca, D., Shiner, P., Zucconi, V., 2004. Applying thick-skinned tectonic models to the Apennine thrust belt of Italy: limitations and implications. In: McClay, K.R. (Ed.), Thrust Tectonics and Petroleum Systems. A.A.P.G. Memoir. 82, pp. 647–667.
Caiazzo, C., Ascione, A., Cinque, A., 2006. Late Tertiary-Quaternary tectonics of the southern Apennines (Italy): new evidences from the Tyrrhenian slope. Tectonophysics 421, 23–51.
Candela, S., Mazzoli, S., Megna, A., Santini, S., 2015. Finite element modelling of stress field perturbations and interseismic crustal deformation in the Val d'Agri region, southern Apennines, Italy. Tectonophysics 657, 245–259.
Capalbo, A., Ascione, A., Aucelli, P.P.C., Mazzoli, S., 2010. Evaluation of the erosion rate in the southern Apennines (Italy) based on geological-geomorphological data. Il Quaternario 23, 75–90.
Cello, G., Mazzoli, S., 1998. Apennine tectonics in southern Italy: a review. J. Geodyn. 27, 191–211.
Cello, G., Guerra, I., Tortorici, L., Turco, E., Scarpa, R., 1982. Geometry of the neotectonic stress field in southern Italy: geological and seismological evidence. J. Struct. Geol. 4, 385–393.
Cello, G., Invernizzi, C., Mazzoli, S., Tondi, E., 2001. Fault properties and fluid flow patterns from Quaternary faults in the Apennines, Italy. Tectonophysics 336, 63–78.
Cello, G., Tondi, E., Micarelli, L., Mattioni, L., 2003. Active tectonics and earthquake sources in the epicentral area of the 1857 Basilicata earthquake (Southern Italy). J. Geodyn. 36, 37–50.
Cinque, A., Patacca, E., Scandone, P., Tozzi, M., 1993. Quaternary kinematic evolution of the Southern Apennines. Relationships between surface geological features and deep lithospheric structures. Ann. Geophys. 36, 249–260.
Ciotoli, G., Lombardi, S., Annunziatellis, A., 2007. Geostatistical analysis of soil gas data in a high seismic intermontane basin: Fucino Plain, central Italy. J. Geophys. Res. 112, B05407.
Clark, M.K., Schoenbohm, L.M., Royden, L.H., Whipple, K.X., Burchfiel, B.C., Zhang, X., Tang, W., Wang, E., Chen, L., 2004. Surface uplift, tectonics, and erosion of eastern Tibet from large-scale drainage patterns. Tectonics 23, TC1006. http://dx.doi.org/10.1029/2002TC001402.
Colella, A., Lapenna, V., Rizzo, E., 2004. High-resolution imaging of the High Agri Valley Basin (Southern Italy) with electrical resistivity tomography. Tectonophysics 386, 29–40.
Corrado, S., Invernizzi, C., Mazzoli, S., 2002. Tectonic burial and exhumation in a foreland fold and thrust belt: the Monte Alpi case history (Southern Apennines, Italy). Geodin. Acta 15, 159–177.
Corrado, S., Aldega, L., Di Leo., P., Giampaolo, C., Invernizzi, C., Mazzoli, S., Zattin, M., 2005. Thermal maturity of the axial zone of the southern Apennines fold-and-thrust belt (Italy) from multiple organic and inorganic indicators. Terra Nova 17, 56–65.
Cowie, P.A., Roberts, G.P., 2001. Constraining slip rates and spacings for active normal faults. J. Struct. Geol. 23, 1901–1915.
Cowie, P.A., Gupta, S., Dawers, N.H., 2000. Implications of fault array evolution for synrift depocentre development: insights from a numerical fault growth model. Basin Res. 12, 241–261.
D'Agostino, N., Jackson, J.A., Dramis, F., Funiciello, R., 2001. Interactions between mantle upwelling, drainage evolution and active normal faulting: an example from the central Apennines (Italy). Geophys. J. Int. 147, 475–497.
Demoulin, A., 1998. Testing the tectonic significance of some parameters of longitudinal river profiles: the case of the Ardenne (Belgium, NW Europe). Geomorphology 24, 189–208.
Devoti, R., Esposito, A., Pietrantonio, G., Pisani, A.R., Riguzzi, F., 2011. Evidence of large scale deformation patterns from GPS data in the Italian subduction boundary. Earth Planet. Sci. Lett. 311, 230–241.
Di Biase, R.A., Whipple, K.X., 2011. The influence of erosion thresholds and runoff variability on the relationships among topography, climate and erosion rate. J. Geophys. Res. 116, F04036. http://dx.doi.org/10.1029/2011JF002095.
Di Niro, A., Giano, S.I., Santangelo, N., 1992. Primi dati sull'evoluzione geomorfologica e sedimentaria del bacino dell'alta Val d'Agri (Basilicata). Studi Geol. Camerti 1, 257–263.
Duvall, A., Kirby, E., Burbank, D., 2004. Tectonic and lithologic control on bedrock channel profiles and processes in coastal California. J. Geophys. Res. 109, F03002. http://dx.doi.org/10.1029/2003JF000086.
Faccenna, C., Davy, P., Brun, J.-P., Funiciello, R., Giardini, D., Mattei, M., Nalpas, T., 1996. The dynamics of back-arc extension: an experimental approach to the opening of the Tyrrhenian Sea. Geophys. J. Int. 126, 781–795.
Faccenna, C., Mattei, M., Funiciello, R., Jolivet, L., 1997. Styles of back-arc extension in the Central Mediterranean. Terra Nova 9, 126–130.
Faure Walker, J.P., Roberts, G.P., Cowie, P.A., Papanikolau, I.D., Michetti, A.M., Sammonds, P.R., Wilkinson, M., McCaffrey, K.J.W., Phillips, R.J., 2012. Relationships between topography, rates of extension and mantle dynamics in the actively-extending Italian Apennines. Earth Planet. Sci. Lett. 325, 76–84.
Filocamo, F., Romano, P., Di Donato, V., Esposito, P., Mattei, M., Porreca, M., Robustelli, G., Russo Ermolli, E., 2009. Geomorphology and tectonics of uplifted coasts: new chronostratigraphical constraints for the Quaternary evolution of Tyrrhenian North Calabria (southern Italy). Geomorphology 105, 334–354.
Filocamo, F., Ascione, A., Romano, P., 2010. The marine terraces of the Policastro Gulf: new insights on the evolution of the Southern Apennines Tyrrhenian margin. Rend. Online Soc. Geol. Ital. 11, 40–41.
Flint, J.J., 1974. Stream gradient as a function of order, magnitude and discharge. Water Resour. Res. 10, 969–973.
Forte, A.M., Whipple, K.X., Cowgill, E., 2015. Drainage network reveals patterns and history of active deformation in the eastern Greater Caucasus. Geosphere 11, 1343–1364.
Frepoli, A., Amato, A., 2000. Fault plane solutions of crustal earthquakes in Southern Italy (1988–1995): seismotectonic implications. Ann. Geophys. 43, 437–467.
Galli, P., Molin, D., Camassi, R., Castelli, V., 2001. Il terremoto del 9 settembre 1998 nel quadro della sismicità storica del confine Calabro-Lucano. Possibili implicazioni sismotettoniche. Il Quaternario Ital. 14, 31–40.
Galli, P., Bosi, V., Piscitelli, S., Giocoli, A., Scionti, V., 2006. Late Holocene earthquakes in southern Apennine: paleoseismology of the Caggiano fault. Int. J. Earth Sci. 95, 855–870.
Giano, S.I., Giannandrea, P., 2014. Late Pleistocene differential uplift inferred from the analysis of fluvial terraces (southern Apennines, Italy). Geomorphology 217, 89–105.
Giano, S.I., Maschio, L., Alessio, M., Ferranti, L., Improta, S., Schiattarella, M., 2000. Radiocarbon dating of active faulting in the Agri high valley, southern Italy. J. Geodyn. 29, 371–386.
Gilchrist, A.R., Kooi, H., Beaumont, C., 1994. Post-Gondwana geomorphic evolution of southwestern Africa: implications for the controls on landscape development from observations and numerical experiments. J. Geophys. Res. 99, 12,211–12,228.
Hack, J.T., 1957. Studies of longitudinal stream profiles in Virginia and Maryland. U.S. Geol. Surv. Prof. Pap. 249-B, 45–97.
Hippolyte, J.-C., Angelier, J., Roure, F., 1994. A major geodynamic change revealed by Quaternary stress patterns in the southern Apennines (Italy). Tectonophysics 230, 199–210.
Howard, A.D., 1994. A detachment-limited model of drainage basin evolution. Water Resour. Res. 30, 2261–2285. http://dx.doi.org/10.1029/94WR00757.
I.S.P.R.A., d. Note illustrative della Carta Geologica d'Italia alla scala 1:50.000, Foglio 521 'Lauria'. I.S.P.R.A. - Servizio Geologico d'Italia, Romahttp://www.isprambiente.gov.it/Media/carg/basilicata.html (in press).
Iannace, A., Vitale, S., D'Errico, M., Mazzoli, S., Di Staso, A., Macaione, E., Messina, A., Reddy, S.M., Somma, R., Zamparelli, V., Zattin, M., Bonardi, G., 2007. The carbonate tectonic units of northern Calabria (Itlay): a record of Apulian paleomargin evolution and Miocene convergence, continental crust subduction, and exhumation of HP-LT rocks. J. Geol. Soc. Lond. 164, 1165–1186.
Invernizzi, C., Bigazzi, G., Corrado, S., Di Leo, P., Schiattarella, M., Zattin, M., 2008. New thermobaric constraints on the exhumation history of the Liguride accretionary wedge, southern Italy. Ofioliti 33, 21–32.

Kastens, K., Mascle, J., Auroux, C., Bonatti, E., Broglia, C., Channell, J., Curzi, P., Emeis, K.-C., Glaçon, G., Hasegawa, S., Hieke, W., Mascle, G., McCoy, F., McKenzie, J., Mendelson, J., Müller, C., Réhault, J.-P., Robertson, A., Sartori, R., Sprovieri, R., Torii, M., 1988. ODP Leg 107 in the Tyrrhenian Sea: insights into passive margin and back-arc basin evolution. Geol. Soc. Am. Bull. 100, 1140–1156.
Kerrich, R., 1986. Fluid infiltration into fault zones: chemical, isotopic and mechanical effects. Pure Appl. Geophys. 124, 225–268.
Kirby, E., Whipple, K., 2001. Quantifying differential rock-uplift rates via stream profile analysis. Geology 29, 415–418.
Kirby, E., Whipple, K.X., 2012. Expression of active tectonics in erosional landscapes. J. Struct. Geol. 44, 54–75.
Kirby, E., Whipple, K.X., Tang, W., Chen, Z., 2003. Distribution of active rock uplift along the eastern margin of the Tibetan Plateau: inferences from bedrock channel longitudinal profiles. J. Geophys. Res. 108. http://dx.doi.org/10.1029/2001JB000861.
Korup, O., Densmore, A.L., Schlunegger, F., 2010. The role of landslides in mountain range evolution. Geomorphology 120, 77–90.
La Rocca, S., Santangelo, N., 1991. Primi dati sull'evoluzione geomorfologica del bacino lacustre del F. Noce (Basilicata). Geogr. Fis. Din. Quat. 14, 229–242.
Lavé, J., Avouac, J.P., 2001. Fluvial incision and tectonic uplift across the Himalayas of central Nepal. J. Geophys. Res. 106, 26,561–26,591.
Macchiavelli, C., Mazzoli, S., Megna, A., Saggese, F., Santini, S., Vitale, S., 2012. Applying the multiple inverse method to the analysis of earthquake focal mechanism data: new insights into the active stress field of Italy and surrounding regions. Tectonophysics 580, 124–149. http://dx.doi.org/10.1016/j.tecto.2012.09.007.
Malinverno, A., Ryan, W.B.F., 1986. Extension in the Tyrrhenian Sea and shortening in the Apennines as result of arc migration driven by sinking of the lithosphere. Tectonics 5, 227–245.
Mattei, M., Petrocelli, V., Lacava, D., Schiattarella, M., 2004. Geodynamic implications of Pleistocene ultrarapid vertical-axis rotations in the southern Apennines, Italy. Geology 32, 789–792.
Mazzoli, S., Barkham, S., Cello, G., Gambini, R., Mattioni, L., Shiner, P., Tondi, E., 2001. Reconstruction of continental margin architecture deformed by the contraction of the Lagonegro Basin, southern Apennines, Italy. J. Geol. Soc. Lond. 158, 309–319.
Mazzoli, S., Aldega, L., Corrado, S., Invernizzi, C., Zattin, M., 2006. Pliocene-quaternary thrusting, syn-orogenic extension and tectonic exhumation in the Southern Apennines (Italy): insights from the Monte Alpi area. Geol. Soc. Am. Spec. Pap. 414, 55–77.
Mazzoli, S., D'Errico, M., Aldega, L., Corrado, S., Invernizzi, C., Shiner, P., Zattin, M., 2008. Tectonic burial and 'young' (<10 Ma) exhumation in the southern Apennines fold-and-thrust belt (Italy). Geology 36, 243–246. http://dx.doi.org/10.1130/G24344A.
Mazzoli, S., Szaniawski, R., Mittiga, F., Ascione, A., Capalbo, A., 2012. Tectonic evolution of Pliocene-Pleistocene wedge-top basins of the southern Apennines: new constraints from magnetic fabric analysis. Can. J. Earth Sci. 49, 492–509. http://dx.doi.org/10.1139/E11-067.
Mazzoli, S., Ascione, A., Buscher, J.T., Pignalosa, A., Valente, E., Zattin, M., 2014. Low-angle normal faulting and focused exhumation associated with late Pliocene change in tectonic style in the southern Apennines (Italy). Tectonics 33, 1802–1818. http://dx.doi.org/10.1002/2014TC003608.
Merritts, D., Vincent, K.R., 1989. Geomorphic response of coastal streams to low, intermediate and high rates of uplift, Mendocino triple junction region, northern California. Geol. Soc. Am. Bull. 101, 1373–1388.
Michetti, A.M., Ferreli, L., Serva, L., Vittori, E., 1997. Geological evidence for strong historical earthquakes in an "aseismic" region: the Pollino case (Southern Italy). J. Geodyn. 24, 67–86.
Michetti, A.M., Ferreli, L., Esposito, E., Porfido, S., Blumetti, A.M., Vittori, E., Serva, L., Roberts, G.P., 2000. Ground effects during the 9 September 1998, $M_w = 5.6$ Lauria earthquake and the seismic potential of the "aseismic" Pollino region in southern Italy. Seismol. Res. Lett. 71, 31–46.
Miller, S.R., Slingerland, R.L., 2006. Topographic advection on fault-bend folds: inheritance of valley positions and the formation of wind gaps. Geology 34, 769–772.
Minissale, A., 2004. Origin, transport and discharge of CO_2 in central Italy. Earth-Sci. Rev. 66, 89–141.
Molnar, P., England, P., 1990. Late Cenozoic uplift of mountain ranges and global climate change: chicken or egg? Nature 346, 29–34.
Montgomery, D.R., Foufoula-Georgiou, E., 1993. Channel network source representation using digital elevation models. Water Resour. Res. 29, 3925–3934.
Montone, P., Amato, A., Pondrelli, S., 1999. Active stress map of Italy. J. Geophys. Res. 104, 25,595–25,610.
Morandi, S., Ceragioli, E., 2002. Integrated interpretation of seismic and resistivity images across the "Val d'Agri" graben (Italy). Ann. Geophys. 45 (2), 259–271.
Ouimet, W.B., Whipple, K.X., Royden, L.H., Sun, Z., Chen, Z., 2007. The influence of large landslides on river incision in a transient landscape: eastern margin of the Tibetan Plateau (Sichuan, China). Geol. Soc. Am. Bull. 119, 1462–1476.
Pantosti, D., Valensise, G., 1988. La faglia sud-appenninica: identificazione oggettiva di un lineamento sismogenetico nell'Appennino meridionale. Proc. VII Meet. Gruppo Nazionale di Geofisical della Terra Solida, Rome, pp. 205–220.
Papanikolaou, I.D., Roberts, G.P., 2007. Geometry, kinematics and deformation rates along the active normal fault system in the southern Apennines: implications for fault growth. J. Struct. Geol. 29, 166–188.
Patacca, E., Scandone, P., 2001. Late thrust propagation and sedimentary response in the thrust- belt-foredeep system of the Southern Apennines (Pliocene-Pleistocene). In: Vai, G.B., Martini, I.P. (Eds.), Anatomy of an Orogen: The Apennines and Adjacent Mediterranean Basins. Kluwer Academic Publishers, London, pp. 401–440.
Patacca, E., Sartori, R., Scandone, P., 1990. Tyrrhenian basin and Apenninic arcs: kinematic relations since late Tortonian times. Mem. Soc. Geol. Ital. 45, 425–451.
Pelletier, J.D., 2004. Persistent drainage migration in a numerical landscape evolution model. Geophys. Res. Lett. 31. http://dx.doi.org/10.1029/2004GL020802.
Perron, J.T., Richardson, P.W., Ferrier, K.L., Lapôtre, M., 2012. The root of branching river networks. Nature 492, 100–103. http://dx.doi.org/10.1038/nature11672.
Petrosino, P., Russo Ermolli, E., Donato, P., Jicha, B., Robustelli, G., Sardella, R., 2014. Using tephrocronology and palynology to date the MIS 13 lacustrine sediments of the Mercure basin (Southern Apennines - Italy). Ital. J. Geosci. 133, 169–186. http://dx.doi.org/10.3301/IJG.2013.22.
Pierdominici, S., Heidbach, O., 2012. Stress field of Italy – mean stress orientation at different depths and wave-length of the stress pattern. Tectonophysics 532, 301–311.
Prince, P.S., Spotila, J.A., Henika, W.S., 2011. Stream capture as driver of transient landscape evolution in a tectonically quiescent setting. Geology 39, 823–826. http://dx.doi.org/10.1130/G32008.1.
Ramsey, L.A., Walker, R.T., Jackson, J., 2007. Geomorphic constraints on the active tectonics of southern Taiwan. Geophys. J. Int. 170, 1357–1372.
Robustelli, G., Russo Ermolli, E., Petrosino, P., Jicha, B., Sardella, R., Donato, P., 2014. Tectonic and climatic control on geomorphological and sedimentary evolution of the Mercure basin, southern Apennines, Italy. Geomorphology 214, 423–435. http://dx.doi.org/10.1016/j.geomorph.2013.02.026.
Roe, G.H., Montgomery, D.R., Hallett, B., 2003. Orographic precipitation and the relief of mountain ranges. J. Geophys. Res. 108, 2315. http://dx.doi.org/10.1029/2001JB001521.
Rovida, A., Camassi, R., Gasperini, P., Stucchi, M. (Eds.), 2011. Catalogo Parametrico dei Terremoti Italiani, 2011 version (CPTI11), INGV, Milano, Bologna. http://dx.doi.org/10.6092/INGV.IT[HYPHEN]CPTI11.
Sabato, L., Bertini, A., Masini, F., Albianelli, A., Napoleone, G., Pieri, P., 2005. The lower and middle Pleistocene geological record of the San Lorenzo lacustrine succession in the Sant'Arcangelo Basin (Southern Apennines, Italy). Quat. Int. 131, 59–69.
Salustri Galli, C., Torrini, A., Doglioni, C., Scrocca, D., 2002. Divide and highest mountains vs subduction in the Apennines. Studi Geol. Camerti 1, 143–153.
Santangelo, N., 1991. Evoluzione geomorfologica e stratigrafica di alcuni bacini lacustri del confine campano-lucano (Italia meridionale). PhD Thesis, Università degli Studi di Napoli "Federico II", Napoli (109 pp).
Santangelo, M., Gioia, D., Cardinali, M., Guzzetti, F., Schiattarella, M., 2013. Interplay between mass movement and fluvial network organization: an example from southern Apennines, Italy. Geomorphology 188, 54–67.
Santo, A., Ascione, A., Del Prete, S., Di Crescenzo, G., Santangelo, N., 2011. Collapse sinkholes distribution in the carbonate massifs of central and southern Apennines. Acta Carsol. 40, 95–112.
Sartori, R., 1990. In: Kastens, K.A., Mascle, J., et al. (Eds.), The main results of ODP Leg 107 in the frame of Neogene to Recent geology of PeriTyrrhenian areas. Proceedings of the Ocean Drilling Program, Scientific Results. 107, College Station, TX (Ocean Drilling Program), pp. 715–730.
Savelli, C., Schreider, A.A., 1991. The opening processes in the deep Tyrrhenian basins of Marsili and Vavilov, as deduced from magnetic and chronological evidence of their igneous crust. Tectonophysics 190, 119–131.
Schiattarella, M., 1998. Quaternary tectonics of the Pollino Ridge, Calabria-Lucania boundary, Southern Italy. In: Holdsworth, R.E., Strachan, R.A., Dewey, J.F. (Eds.), Continental Transpressional and Transtensional TectonicsJ. Geol. Soc. Lond. Vol. 135. Special Publications, pp. 341–354.
Schiattarella, M., Di Leo, P., Beneduce, P., Giano, S.I., 2003. Quaternary uplift vs tectonic loading: a case study from the Lucanian Apennine, southern Italy. Quat. Int. 101–102, 239–251.
Schiattarella, M., Di Leo, P., Beneduce, P., Giano, S.I., Martino, C., 2006. Tectonically driven exhumation of a young orogen: an example from the southern Apennines, Italy. Geol. Soc. Am. Spec. Paper 398, 371–385.
Scrocca, D., Carminati, E., Doglioni, C., 2005. Deep structure of the southern Apennines, Italy: thin-skinned or thick-skinned? Tectonics 24, TC3005. http://dx.doi.org/10.1029/2004TC001634.
Sgrosso, I., 1988. Nuovi dati biostratigrafici sul Miocene del Monte Alpi (Lucania) e conseguenti ipotesi paleogeografiche. Mem. Soc. Geol. Ital. 41, 343–351.
Shiner, P., Beccacini, A., Mazzoli, S., 2004. Thin-skinned versus thick-skinned structural models for Apulian carbonate reservoirs: constraints from the Val d'Agri fields, S Apennines, Italy. Mar. Pet. Geol. 21, 805–827.
Sibson, R.H., 2000. Fluid involvement in normal faulting. J. Geodynamics. 29, 469–499.
Sklar, L., Dietrich, W.E., 1998. River longitudinal profiles and bedrock incision models: stream power and the influence of sediment supply. In: Tinkler, K.J., Wohl, E.E. (Eds.), Rivers Over Rock: Fluvial Processes in Bedrock ChannelsGeophys. Monogr. Ser 107. AGU, Washington, D.C., pp. 237–260. http://dx.doi.org/10.1029/GM107p0237.
Snyder, N.P., Whipple, K.X., Tucker, G.E., Merritts, D.J., 2000. Landscape response to tectonic forcing: digital elevation model analysis of stream profiles in the Mendocino triple junction region, northern California. Geol. Soc. Am. Bull. 112, 1250–1263.
Spagnolo, M., Pazzaglia, F.J., 2005. Testing the geological influences on the evolution of river profiles: a case from the Northern Apennines (Italy). Geogr. Fis. Din. Quat. 28, 103–113.
Spina, V., Tondi, E., Galli, P., Mazzoli, S., Cello, G., 2008. Quaternary fault segmentation and interaction in the epicentral area of the 1561 earthquake (Mw = 6.4), Vallo di Diano, southern Apennines, Italy. Tectonophysics 453, 233–245.
Spotila, J.A., 2012. Influence of drainage divide structure on the distribution of mountain peaks. Geology 40, 855–858.
Stark, C.P., 2010. Oscillatory motion of drainage divides. Geophys. Res. Lett. 37, L04401. http://dx.doi.org/10.1029/2009GL040851.
Stock, J., Dietrich, W.E., 2003. Valley incision by debris flows: evidence of a topographic signature. Water Resour. Res. 39, 1089. http://dx.doi.org/10.1029/2001WR001057.
Stock, J.D., Dietrich, W.E., 2006. Erosion of steepland valleys by debris flows. Geol. Soc. Am. Bull. 118, 1125–1148.

Summerfield, M.A., 1991. Global Geomorphology: An Introduction to the Study of Landforms. Longman Sci. and Tech., London (537 pp).
Tarquini, S., Isola, I., Favalli, M., Mazzarini, F., Bisson, M., Pareschi, M.T., Boschi, E., 2007. TINITALY/01: a new triangular irregular network of Italy. Ann. Geophys. 50, 407–425.
Tarquini, S., Vinci, S., Favalli, M., Doumaz, F., Fornaciai, A., Nannipieri, L., 2012. Release of a 10-m-resolution DEM for the Italian territory: comparison with global-coverage DEMs and anaglyph-mode exploration via the web. Comput. Geosci. 38, 168–170. http://dx.doi.org/10.1016/j.cageo.2011.04.018.
Toutain, J.-P., Baubron, J.-C., 1999. Gas geochemistry and seismotectonics: a review. Tectonophysics 304, 1–27.
Tucker, G.E., Slingerland, R.L., 1994. Erosional dynamics, flexural isostasy, and long-lived escarpments: a numerical modeling study. J. Geophys. Res. 99, 12,229–12,243.
Tucker, G.E., Slingerland, R., 1996. Predicting sediment flux from fold and thrust belts. Basin Res. 8, 329–349.
Tucker, G.E., Whipple, K.X., 2002. Topographic outcomes predicted by stream erosion models: sensitivity analysis and intermodal comparison. J. Geophys. Res. 107, 2179. http://dx.doi.org/10.1029/2001JB000162.
Long-term morphotectonic evolution of the Southern Apennines. In: Valente, E. (Ed.), PhD Thesis, Università di Napoli "Federico II", Napoli http://www.fedoa.unina.it/4168/ (224 pp).
Villani, F., Pierdominici, S., 2010. Late Quaternary tectonics of the Vallo di Diano basin (southern Apennines, Italy). Quat. Sci. Rev. 29, 3167–3183.
Whipple, K.X., 2001. Fluvial landscape response time: how plausible is steady-state denudation? Am. J. Sci. 301, 313–325.
Whipple, K.X., 2004. Bedrock rivers and the geomorphology of active orogens. Annu. Rev. Earth Planet. Sci. 32, 151–185.
Whipple, K.X., Tucker, G.E., 1999. Dynamics of stream-power river incision model: implications for height limits of mountain ranges, landscape response timescales, and research needs. J. Geophys. Res. 104, 17,661–17,674.
Whipple, K.X., Tucker, G.E., 2002. Implications of sediment-flux-dependent river incision models for landscape evolution. J. Geophys. Res. 107, 2039. http://dx.doi.org/10.1029/2000JB000044.
Whipple, K.X., Kirby, E., Brocklehurst, S.H., 1999. Geomorphic limits to climate-induced increases in topographic relief. Nature 401, 39–43.
Whipple, K., Wobus, C., Crosby, B., Kirby, E., Sheehan, D., 2007. New Tools for Quantitative Geomorphology: Extraction and Interpretation of Stream Profiles from Digital Topographic Data. Short Course Presented at Geological Society of America Annual Meeting, Denver, CO. Available at http://www.geomorphtools.org.
Whittaker, A.C., 2012. How do landscapes record tectonics and climate? Lithosphere 4, 160–164. http://dx.doi.org/10.1130/RF.L003.1.
Whittaker, A.C., Attal, M., Cowie, P.A., Tucker, G.E., Roberts, G., 2008. Decoding temporal and spatial patterns of fault uplift using transient river long profiles. Geomorphology 100, 506–526. http://dx.doi.org/10.1016/j.geomorph.2008.01.018.
Willett, S.D., 1999. Orogeny and orography: the effects of erosion on the structure of mountain belts. J. Geophys. Res. 104, 28957–28981.
Willett, S.D., Brandon, M.T., 2002. On steady states in mountain belts. Geology 30, 175–178.
Willett, S.D., Slingerland, R., Hovius, N., 2001. Uplift, shortening and steady state topography in active mountain belts. Am. J. Sci. 301, 455–485.
Willett, S.D., McCoy, S.W., Perron, J.T., Goren, L., Chen, C.Y., 2014. Dynamic reorganization of river basins. Science 343 (6175), 1248765. http://dx.doi.org/10.1126/science.1248765.
Willgoose, G., 1994. A physical explanation for an observed area-slope-elevation relationship for catchments with declining relief. Water Resour. Res. 30, 151–159. http://dx.doi.org/10.1029/93WR01810.
Wobus, C., Whipple, K.X., Kirby, E., Snyder, N., Johnson, J., Spyropolou, K., Crosby, B., Sheehan, D., 2006. Tectonics from topography: Procedures, promise and pitfalls. In: Willett, S.D., Hovius, N., Brandon, M.T., Fisher, D.M. (Eds.), Tectonics, Climate, and Landscape Evolution. Geol. Soc. Am. Special Paper. 398, Penrose Conference Series, pp. 55–74. http://dx.doi.org/10.1130/2006.2398(04).
Working Group CPTI, 2004. Catalogo Parametrico dei Terremoti Italiani, 2004 version (CPTI04), INGV, Bologna. http://dx.doi.org/10.6092/INGV.IT-CPTI04.
Zaprowski, B.J., Pazzaglia, F.J., Evenson, E.B., 2005. Climatic influences on profile concavity and river incision. J. Geophys. Res. 110, F03004. http://dx.doi.org/10.1029/2004JF000138.
Zavala, C., 2000. Stratigraphy and sedimentary history of the Plio-Pleistocene Sant'Arcangelo basin, Southern Apennines, Iatly. Riv. Ital. Paleontol. Stratigr. 106, 399–416.
Zuppetta, A., Russo, M., Mazzoli, S., 2004. Miocene tectonic evolution of the southern Apennine thrust front (Italy): stratigraphic and structural constraints from the eastern Calabria-Lucania borderland area. Geodin. Acta 17. http://dx.doi.org/10.3166/ga.17.141-151.